



HAL
open science

Airborne Release Fraction of Dissolved Materials During the Combustion of Liquids Representative of Nuclear Waste Treatment Process

F.-X. Ouf, M. de Mendonca Andrade, H. Feuchter, S. Duval, C. Volkringer, T. Loiseau, F. Salm, P. Ainé, Laurent Cantrel, A. Gil-Martin, et al.

► **To cite this version:**

F.-X. Ouf, M. de Mendonca Andrade, H. Feuchter, S. Duval, C. Volkringer, et al.. Airborne Release Fraction of Dissolved Materials During the Combustion of Liquids Representative of Nuclear Waste Treatment Process. Nuclear Technology, 2023, 209 (2), pp.169-192. 10.1080/00295450.2022.2129274 . hal-03966723

HAL Id: hal-03966723

<https://hal.science/hal-03966723>

Submitted on 31 Jan 2023

HAL is a multi-disciplinary open access archive for the deposit and dissemination of scientific research documents, whether they are published or not. The documents may come from teaching and research institutions in France or abroad, or from public or private research centers.

L'archive ouverte pluridisciplinaire **HAL**, est destinée au dépôt et à la diffusion de documents scientifiques de niveau recherche, publiés ou non, émanant des établissements d'enseignement et de recherche français ou étrangers, des laboratoires publics ou privés.



Distributed under a Creative Commons Attribution - NonCommercial 4.0 International License

Airborne release fraction of dissolved materials during the combustion of liquids representatives of nuclear waste treatment process.

F.-X. Ouf^{a, b}, M. De Mendonca Andrade^a, H. Feuchter^c, S. Duval^c, C. Volkringer^{c, d}, T. Loiseau^c, F. Salm^a, P. Ainé^e, L. Cantrel^a, A. Gil-Martin^e, F. Hurel^f, C. Lavalette^e, P. March^a, P. Nerisson^a, J. Nos^e, and L. Bouilloux^a

^aInstitut de Radioprotection et de Sûreté Nucléaire (IRSN), PSN-RES/SCA, PSN-RES/SA2I, PSN-RES/SEREX, Gif-Sur-Yvette, 91192, France.

^bCurrent affiliation: Laboratoire National de métrologie et d'Essais, Direction de la Métrologie Scientifique et Industrielle, ZA Trappes-Elancourt 29 Rue Roger Hennequin, 78190 Trappes, France

^cUniversité de Lille, CNRS, Centrale Lille, ENSCL, Univ. Artois, UMR 8181 - UCCS - Unité de Catalyse et Chimie du Solide, F-59000 Lille, France.

^dInstitut Universitaire de France (IUF), 1, rue Descartes, 75231 Paris cedex 05, France.

^eOrano, 125 Avenue de Paris, 92320 Châtillon, France.

^fAREXIS Falandre 61380 Mahéru, France.

Corresponding author: frax.ouf@gmail.com

Abstract

Experimental results are reported on the airborne release, under fire conditions, of hazardous materials dissolved in mixture of organic solvents (tributylphosphate TBP and hydrogenated tetrapropylene HTP) representatives of the nuclear fuel recycling process. Cerium and ruthenium have been considered respectively as stable and volatile fission products and which could be eventually released as airborne particles during thermal degradation of contaminated and inflammable liquids. Airborne release fractions (ARF) and their experimental uncertainties have been determined. Considering fire involving contaminated organic solvents, higher ARF are reported for ruthenium Ru(+III) (0.99 +/- 1.20 %) in comparison with cerium (0.22 +/- 0.31 % and 0.20 +/- 0.28 % for Ce(+III) and Ce(+IV), respectively). This discrepancy is partially due to the volatility of ruthenium formed under these conditions. Considering configurations involving an aqueous nitric acid phase placed below contaminated solvents, boiling of this phase enhances the release of contaminant materials, 1.78 +/- 1.06 % and 1.01 +/- 1.31 % for Ce(+III) and Ce(+IV), respectively and 12.41 +/- 29.45 % for Ru(+III). Analysis of size distribution, morphology and chemical composition of released particles and droplets emitted during HTP/TBP bubble collapse are reported, highlighting the contribution of bubble bursting at the solvent surface to airborne release.

Keywords: aerosol released, PUREX, combustion, particle analysis, bubbles bursting.

1. Introduction

Nuclear fuel reprocessing is of prime importance to reduce volume of stored highly radioactive materials and to recycle valuable materials for further processing of mixed oxides. Among the different chemical elements composing nuclear used fuel, uranium and plutonium are critical and need to be purified by liquid-liquid extraction. Several methods have been developed to allow such extraction and among them, the Plutonium Uranium Reduction Extraction (PUREX) reprocessing technique is mainly used in the nuclear industry for specific extraction of Pu(+IV) and U(+VI) from nitric acid solutions ¹. Within this process, extraction is carried out using Tributylphosphate (TBP) in combination with diluents such as hydrogenated tetrapropylene (HTP) or kerosene. In France, the reprocessing plant at La Hague (UP2/UP3 reprocessing plants) has considered HTP diluent and reprocesses nearly 1 700 metric tonnes of heavy metal per year ¹. Due to high flammability of those organic solvents and past fire events reported in commercial nuclear industry ², special care regarding explosion and fire risks must be considered during safety analysis of nuclear fuel reprocessing facilities. Beyond the question of

53 direct consequences of fires on containment devices by soot emissions ^{3,4}, their transport in facility rooms and
54 ventilation networks ^{5,6} and their direct contribution to clogging of high efficiency particulate air filters (HEPA)
55 by emitted particles ⁷⁻⁹, resuspension of radioactive material under aerosol form must be considered for estimating
56 source terms potentially released ¹⁰⁻¹⁴.

57 Prediction of consequences of fires within industrial facility handling hazardous materials is generally based on
58 the airborne release fraction describing the ability of contaminants to be dispersed as airborne particles according
59 to an external stress. For the specific hypothetical case of fire occurring during the PUREX process, the airborne
60 release fraction ARF is defined as the ratio between the mass of hazardous material released in airborne phase
61 (m_{released}) and the mass of the same hazardous material initially dissolved within contaminated liquids (m_{initial}):

$$62 \quad \text{ARF} = \frac{m_{\text{released}}}{m_{\text{initial}}} \quad (\text{Eq. 1})$$

63
64
65 For safety reasons, it is crucial to be able to predict the order of magnitude of ARF. Nevertheless, due to complexity
66 of chemical processes induced by extraction in the PUREX process, but also during the pyrolysis of HTP/TBP
67 solvents, current state of knowledge of the scientific community still remains limited from a phenomenological
68 point of view.

69 Several studies have been conducted in the past regarding releases of radioactive materials from burning of
70 HTP/TBP contaminated solutions. Table I presents a review of experimental conditions associated to previous
71 works conducted both at an analytical scale, i.e. less than half a liter ¹⁴⁻²²) and at a larger scale, from several liters
72 to pool fires with a surface lower than 1 m² ^{15,16,19} to nearly 200 L and pool surface reaching up to 5 m² ^{16,19,20,23-25}.
73 Results obtained by Malet et al., (1983) ¹⁹ are also reported in Table I. Due to potential errors in the interpretation
74 of data presented in this study (especially regarding the definition of “Transfer coefficient”), values reported in
75 this study will not be considered in the rest of our analysis and discussion of literature.

76 Analysis of Table I highlights a significant variation, in terms of ARF, mainly due to different types and
77 concentrations of contaminants (elements present in the nuclear fuel), but also to experimental protocols and
78 scales.

79 Dealing with any potential scale effects, mean values of ARF could be computed by considering non-volatiles
80 contaminants (and as a consequence by excluding values reported for Cs, Ru and I in Table I). Comparison of
81 mean ARF values (associated to a confidence interval (CI) of 95% and presented hereafter by considering extended
82 absolute standard deviation (k=2)) of 0.2 +/- 0.2 % ^{14,16,18,26,27} and 1.7 +/- 4.5 % ^{16,24,25} for small (< 0.4 m²) and
83 large (> 0.4 m²) scale pool fires, respectively, do not highlight any statistical differences and, consequently, no
84 influence of pool size on aerosol release fraction. Limit of 0.4 m² for characterizing small scale pool fires
85 (corresponding to an effective pool diameter of 0.7 m) has been considered based on previous studies on scale
86 effect on smoke yield ²⁸ and mass loss rate ²⁹. One must notice that the reported order of magnitudes, for both
87 small and large scales, are consistent with a conservative ARF value of 10 %, commonly recommended for this
88 type of fire scenario ^{10,30}.

89 Considering the contaminants nature, obviously, their volatility has a significant effect on aerosol resuspension.
90 In this context, the question of ruthenium volatility has been addressed by several authors ^{15,16} while the highest
91 ARF was reported for gaseous iodine with a mean value of 77.2% +/- 18.2 % for a confidence interval of 95% ²³.
92 Beyond the question of volatility, other non-volatile elements (Ce, Sr, Zr and U) are generally characterized by
93 significantly smaller order of magnitude of ARF (from 0.002 % to 58.6 % with a mean value of 4.6% +/- 25.2%
94 for a confidence interval of 95%) without any specific trend regarding the nature of elements. On the other hand,
95 influence of several contaminant concentrations on ARF was investigated in the literature. While an increase of U
96 concentration leads to an increase of ARF when using uranium nitrate (mainly associated to the contribution of
97 nitrate to fuel mass loss rate and stronger boiling effect (Ballinger et al., 1988; Jordan & Lindner, 1984)), dispersion

98 and level of uncertainties associated to values reported in the literature do not allow to conclude on any direct
99 effect of contaminant concentrations on ARF.

100 Beyond this wide range of variation of ARF reported in the literature, discussion on the relevance of the surrogate
101 proposed to simulate the chemical and physical behaviour of plutonium complexes formed in the organic phase in
102 terms of aerosol resuspension is limited. As far as we are concerned, no study was able to propose a justified
103 surrogate of plutonium. In some cases, uranium was considered as a proxy of the plutonium to determine
104 experimentally its ARF (Ballinger et al., 1988; Mishima & Schwendiman, 1973c; Nishio & Hashimoto, 1989).
105 On the other hand, other authors have studied fission products under realistic fire conditions but discussion on the
106 relevance of ARF reported for such elements is still missing. Thus, in the present study, both approaches will be
107 considered. The first one will deal with cerium as a chemical surrogate of the plutonium complexes formed in the
108 organic phase of the PUREX process. It is well known that plutonium(IV) forms a tetranitrate complex with the
109 TBP in the form of $(\text{Pu}(\text{NO}_3)_4(\text{TBP})_2)^{31}$ and recent studies were devoted to propose a surrogate, in terms of
110 extraction from an aqueous contaminated phase to a TBP/diluent organic phase of plutonium, to mainly perform
111 experimental measurements of ARF^{31,32} that could be used for predicting plutonium release. Despite the fact that
112 cerium is a fission product encountered in the PUREX process, this element, in the form of CeO_2 , is commonly
113 considered as a surrogate of plutonium dioxide PuO_2 ³³ but also in complexed forms³¹. Dealing with the relevance
114 of Ce(+IV) to mimic the behaviour of Pu(+IV) within the PUREX process, recent studies have highlighted some
115 limitations in the use of cerium since additional hydrated complexes³⁴ could be formed in addition to tetranitrate-
116 TBP complexes and that Ce(+IV) could be reduced to Ce(+III) form, when going from the organic to the aqueous
117 phase³². Nevertheless, in this study and in the present state of the art, cerium was considered as a potential
118 surrogate for plutonium since it is not possible to conduct ARF measurement for Pu due to its high radioactivity
119 and specific handling installation requirements. Then, Cerium was mainly used to investigate release mechanisms
120 and driving forces. On this subject, few studies were devoted to the phenomenological description of contaminant
121 release during contaminated pool fire. Most experimental studies considered bubble bursting induced by pool
122 boiling as the main driven mechanism in contaminant entrainment^{14,15}. More recently, numerical modelling
123 approach was introduced by Brown et al.³⁵⁻³⁷, confirming the significance of the boiling phenomena as one of the
124 most influencing physical mechanism involved in aerosol release from contaminated pool fire. In such a situation,
125 bubbles are expected to present a diameter close to 1-3 mm and their collapses are characterized by droplet
126 emissions with diameter ranging from 1-100 μm and 100-300 μm for film breakup or jet regimes, respectively
127^{36,38}. Additional clues of the significance of bubble bursting on the overall airborne release were introduced by
128 demonstrating the spherical shape of released uranium particles¹⁴ within a size range of nearly 1-10 μm in
129 agreement with a droplet drying process. Nevertheless, and as far as we are concerned, limited number of studies
130 attempted to specifically analyze the size and shape of released particles^{14,15}, and concluded to the occurrence of
131 optical and mass median aerodynamic diameters in the range 1-2 μm and 1-10 μm , respectively. Furthermore,
132 both authors reported isolated and well separated particles, in terms of size, from soot particles emitted by the
133 combustion of solvents. More recently, Hubbard et al.²² reported the release of $\sim 0.2 \mu\text{m}$ spherical lanthanide
134 phosphate particles from 70% kerosene/30% TBP solutions highly contaminated (100 g/L) with hydrated
135 lanthanide nitrates ($\text{Ln}(\text{NO}_3)_3 \cdot 6\text{H}_2\text{O}$).

136 To open the way to a phenomenological model of airborne release of particles from burning contaminated solvents,
137 it is then crucial to characterize the shape and the size of emitted surrogate containing particles. Additional analysis
138 of number and size of bubbles emitted at the surface of the burning liquid is also needed with special attention to
139 the emission of droplets during bubble bursting.

140 The aim of the present study is to propose new experimental findings for linking the properties of released particles
141 with those of bubbles and droplets suspected to be the main cause of contaminant resuspension in the aerosol
142 phase. For this purpose, cerium(+IV) and ruthenium(+III) were both considered as contaminants. Despite
143 previously mentioned limitations, cerium(+IV) will be used to mimic the behaviour of plutonium(+IV) in a
144 complexed form. Ruthenium(+III) will be investigated to analyse the airborne release of an element known to
145 produce volatile form (RuO_4) during fire experiments^{16,39}. In addition to cerium(+IV), and in order to investigate

146 the effect of chemical form of contaminant in the organic phase, cerium(+III) was also considered. ARF were then
147 determined according to a qualified experimental protocol. Additional efforts were also devoted to investigate the
148 nature, shape and size distribution of particles released from cerium and ruthenium contaminated solvents,
149 respectively to support hypothesis both on bubbles bursting and volatile behaviour of ruthenium. In a last step,
150 size of bubbles formed during the combustion of contaminated solvents was characterized prior to the analysis of
151 number and size distribution of film and jet droplets emitted from bubbles generated at an air / liquid HTP-TBP
152 interface under ambient non-flaming conditions.

153 Table I-part 1: analysis of airborne release fractions reported in the literature measured experimentally (white lines) or postulated (grey lines)

Fuel composition (in volume)	Contaminants	Combustion details	Pool size	Mean or range ARF (%) 95 % CI (number of test)	Comments	Reference
70% kerosene/30% TBP	Pu(NO ₃) ₄ 5.4 g/L + UO ₂ (NO ₃) ₂ 11.1 g/L + Th(NO ₃) ₄ 64 g/L + Fission products	100 L of organics air change 0.5–5 h ⁻¹	12.3 m ²	0.12 +/- 0.06 (3)	Modelling approach, airborne release induced by airflow ²³	²⁴
			24.5 m ²	0.31 (3)		
70% HTP / 30% TBP	Dissolved contaminant	All range	All range	10	Recommendations from literature analysis	^{30, 40}
70% normal paraffin hydrocarbon (NPH) / 30% TBP	Uranium 270 g U/L Cesium ~0.2 ppm Cerium ~0.2 ppm Zirconium ~0.2 ppm Iodine ~0.2 ppm	25 ml Forced ventilation	Small scale	U: 0.12 +/- 0.32 (3) Cs: 0.42 +/- 0.78 (4) Ce: 0.70 +/- 0.19 (4) Zr: 0.48 +/- 0.43 (3) I: 77.18 +/- 18.18 (6)	Study of air entrainment Iodine: volatile fission product	²³
70% normal paraffin hydrocarbon (NPH) / 30% TBP	Strontium ~0.2 g Sr/L	150 L	~2.5 m ²	0.21 +/- 0.04 (2)		²⁵
Kerosene + contaminated 5 M HNO ₃	Pu(NO ₃) ₄ in 5M HNO ₃ , 160 g Pu / Kg solution)	< 100 ml kerosene	Small scale	0.026 (1)	No TBP, contamination only in HNO ₃ .	²¹
70% kerosene/30% TBP	Cerium or Thorium at 0.55 g/L in organics (no mention of oxidation state of elements)	20-157 ml Free atmosphere	78 cm ²	TC: 33.57 +/- 27.95 (7) FRF 0.015 (4)	No influence of pool size on ARF TC: transfer coefficient FRF: fraction reaching filter	¹⁹ <i>Not considered in the present analysis</i>
	Cerium in organics (no mention of oxidation state of elements)	20 -250 L Free atmosphere	0.4 - 5 m ²	TC: 58.60 +/- 60.97 (5) FRF: 0.017 (3)		
70% kerosene/30% TBP	Uranium nitrate, 1 g U /L to 84 g U/L	50 ml of organics	33 cm ²	Mean: 1.17 +/- 0.80 (5) Range: 0.7 – 1.6	ARF increases with increasing [U].	²⁰

154

155

156 Table I-part 2: analysis of airborne release fractions reported in the literature measured experimentally (white lines) or postulated (grey lines)

Fuel composition (in volume)	Contaminants	Combustion details	Pool size	Mean or range ARF (%) 95 % CI (number of test)	Comments	Reference
70% normal paraffin hydrocarbon (NPH) / 30% TBP	Uranium nitrate, 1 g U /L to 84 g U/L	50 ml of organics	33 cm ²	Mean: 1.86 +/- 1.11 (10) Range: 0.9 – 2.6	Sphere like U particles, 1-2 μm optical diameter, not connected to soot particles. ARF increases in presence of HNO ₃ .	14
70% normal paraffin hydrocarbon (NPH) / 30% TBP + 3M HNO ₃ : ratio 3:1				Mean: 5.75 +/- 4.63 (6) Range: 3.5 – 9.3 (6)		
70% normal paraffin hydrocarbon (NPH) / 30% TBP + 3M HNO ₃ : ratio 1:1				Mean: 6.25 +/- 7.56 (4) Range: 1.8 – 10.3		
70% normal paraffin hydrocarbon (NPH) / 30% TBP + 3M HNO ₃ : ratio 1:1	Depleted uranium 101.2 g U/L in organics	100 ml of organics Free atmosphere	Small scale	0.47 +/- 0.16 (3)	Presence of fission products limit uranium migration to the acid from the organic phase	18
	Depleted uranium, 101.2 g U /L in organics / fission product in acid			2.61 +/- 0.26 (2)		
	Pure organics, depleted uranium 188 g U/L in acid			6.53 +/- 1.57 (2)		
70% normal paraffin hydrocarbon (NPH) / 30% TBP + 3M HNO ₃ : ratio 1:2	Pure organics, depleted uranium 188 g U/L in acid + fission products	50 ml of organics Free atmosphere	Small scale	0.81 (1)		
70% normal paraffin hydrocarbon (NPH) / 30% TBP + 3M HNO ₃ : ratio 1:3	Depleted uranium, 101.2 g U/L in organics / 188 g U/L in acid + fission products	50 ml of organics Free atmosphere		1.56 (1)		
	Pure organics, depleted uranium 188 g U/L in acid + fission products			0.17 (1)		

157

158 Table I-part 3: analysis of airborne release fractions reported in the literature measured experimentally (white lines) or postulated (grey lines)

Fuel composition (in volume)	Contaminants	Combustion details	Pool size	Mean or range ARF (%) 95 % CI (number of test)	Comments	Reference
70% n-dodecane/30% TBP + water, ratio 1:1	Cerium 8 – 10 g Ce/L Cesium 39 – 64 g Cs/L Ruthenium 2 – 17 g Ru/L Strontium 45 – 118 g Sr/L		0.08 – 0.7 m ²	Ce: 0.17 +/- 0.49 (15) Cs: 10.31 +/- 19.59 (15) Ru: 8.77 +/- 18.05 (18) Sr: 0.26 +/- 0.46 (10)	No influence of pool size on ARF excepted for Sr	16
70% n-dodecane/30% TBP + water with or without HNO ₃	Cerium, Cesium Ruthenium Strontium UO ₂ (NO ₃) ₂ (0.06 – 6 g U/L)	150 ml Air change 30 h ⁻¹	14 cm ²	Cs: 12.54 +/- 16.65 (4) Ru: 7.62 +/- 27.66 (6) Sr: 2.73 +/- 5.87 (4) U: 0.031 +/- 0.046 (8) U w.out HNO ₃ : 3.1E ⁻³ +/- 2.5E ⁻³ (7)	Ru volatility: RuO ₂ (s) + O ₂ (g) => RuO ₄ (g) RuO ₄ (g) + solvent vapor => RuO ₂	
70% HTP / 30 % TBP	~0.5–1 g Ru /L in organics	150 ml of organics Free atmosphere	Small scale	0.67 +/- 0.43 (4)	Slight decrease of ARF with increasing [Ru] No influence of pool size on ARF	15
	2–3.3 g Ru /L in organics	3 – 5 L of organics	0.16 m ²	0.51 +/- 0.63 (4)		
	1.7 g Ru/L in organics	6 L of solvent	0.16 m ²	0.31 (1)		
		Free atmosphere	0.63 m ²	0.49 (1)		
70% HTP / 30 % TBP HNO ₃ at 3M, ratio 1:1	3.3 g Ru /L in organics - pure acid	3 L of organics	0.16 m ²	0.42 +/- 0.30 (2)	No influence of acid	
	~1 g Ru/L organics - ~3 g Ru/L acid	Free atmosphere		0.49 +/- 0.26 (2)		
70% Kerosene / 30 % TBP	100 g/L Lu(NO ₃) ₃ •6H ₂ O 100 g/L Yb(NO ₃) ₃ •6H ₂ O 100 g/L ²³⁸ U(NO ₃) ₂ •6H ₂ O	25 ml of organics 42.5 m ³ /h of airflow in test chamber	Small scale	0.002 +/- 0.003 (3) 0.016 +/- 0.055 (3) 0.102 +/- 0.152 (3)	200 nm spherical Lu/Yb/U phosphates particles. Lu, Yb nitrates precipitation suspected.	22

159

160 **II. Experimental procedure**

161
162 **II.A. Contaminated materials**

163
164 Experiments were conducted by burning previously contaminated 30% tributylphosphate TBP ($C_{12}H_{27}O_4P$,
165 reference A16084 from Alfa Aesar) diluted in 70% hydrogenated tetrapropylene HTP (Novasep Sas, France).
166 Organics solutions were prepared by extraction from nitric acid aqueous solution (HNO_3 at 65%, reference 20429
167 from VWR) containing known concentration of element of interest as a dissolved phase. Concentration of aqueous
168 phase is imposed according to dissolution of known mass of salts containing cerium (for Ce(+IV): Cerium(+IV)
169 Ammonium Nitrate $(NH_4)_2Ce(NO_3)_6$ or CAN, reference 39215.14 from Alfa-Aesar; for Ce(+III): Cerium nitrate
170 hexahydrate $Ce(NO_3)_3 \cdot 6(H_2O)$, reference 218695000 from Acros Organics, for Ce(+III)) and ruthenium
171 (Ruthenium nitrosyl nitrate $RuNO(NO_3)_3$ known for its good extractability within the conditions of the PUREX
172 process, reference 12175 from Alfa Aesar, for Ru(+III)). As previously mentioned, Ce(+IV) was considered as a
173 potential surrogate of Pu(+IV). However, as reported by a previous study³², the reduction of Ce(+IV) into Ce(+III)
174 and backextraction from the organic to the aqueous phase of cerium occurs during combustion. This point has
175 been demonstrated as one the main limitation for the use of Ce(+IV) to mimic the complex behaviour of Pu(+IV)
176 during the solvent combustion and to go further, Ce(+III) was also considered as a contaminant. Final
177 concentrations of these specific elements (Ce or Ru) are then computed according to the composition and purity
178 of these salts. Pure organic and contaminated aqueous phases are put in contact by mixing them in a borosilicate
179 glass settling tank of 1 liter during 5 min when considering cerium solutions and 60 min for ruthenium which is
180 longer due to its lower extractability at ambient temperature (close to 14% from^{41,42}) compared to cerium (higher
181 than 95% from³²). Due to its low extractability and its cost, ruthenium concentration of contaminated solvents
182 was voluntarily fixed at 0.6 Ru g/L (in agreement with the concentration considered in¹⁵). Contaminated organic
183 and aqueous phases were finally separated by gravity. For all conditions, concentrations of Ce and Ru elements
184 have been determined for organic phases by ICP-MS (Inductively Coupled Plasma Mass Spectrometry) analysis
185 and corresponding values have been considered for each test used as reference for computing airborne release
186 fraction. Table II presents experimental conditions for cerium and ruthenium contaminants.

187 Table II: Experimental conditions of different concentrations of cerium(+IV or +III) and ruthenium(+III) in
188 HTP/TBP or HTP/TBP/ HNO_3 mixtures (absolute extended uncertainty for $[C_{org}]$ at a CI of 95 %)

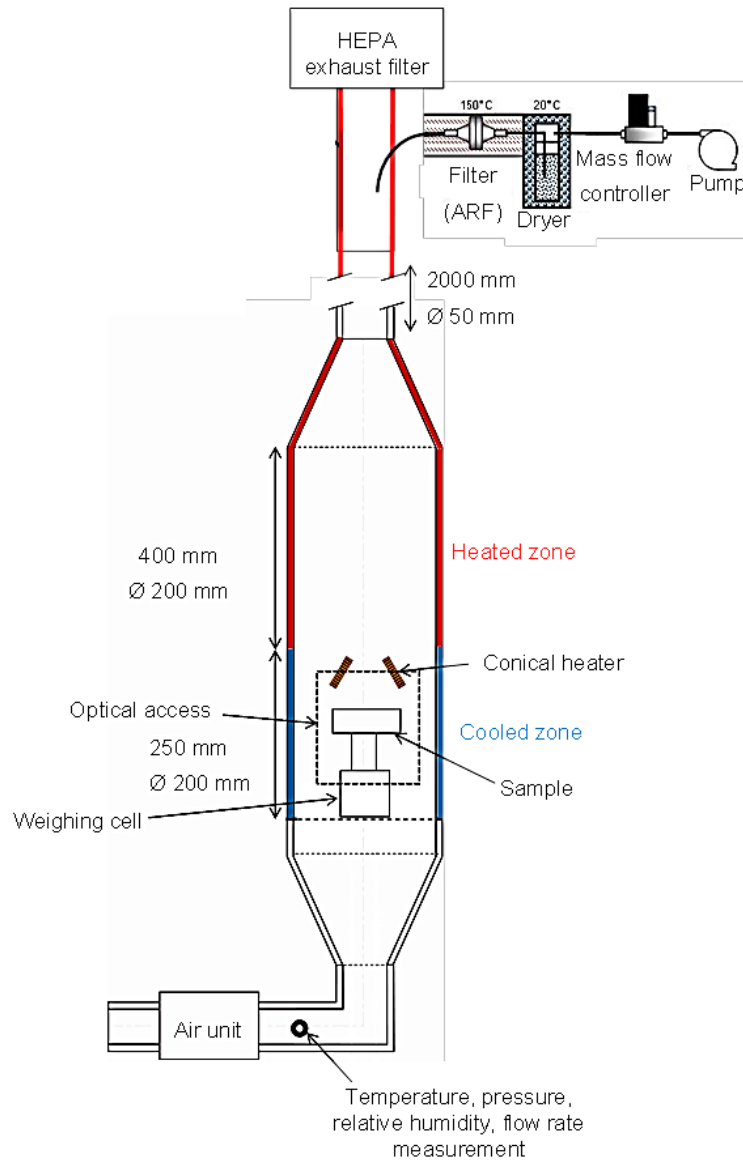
Fuel composition (in volume)	Element	Salt	Number of tests	$[C_{org}]$ (g/L)	V_{org} (ml)	V_{aq} (ml)
Contaminated 70% HTP / 30% TBP	Ce(+III)	Cerium(III) nitrate hexahydrate $Ce(NO_3)_3 \cdot 6(H_2O)$	3	0.2 +/- 0.01	30	-
			3	4.8 +/- 0.05		
			4	9.3 +/- 0.01		
Contaminated 70% HTP / 30% TBP + Pure HNO_3 3M, Ratio 1:1	Ce(+III)	$Ce(NO_3)_3 \cdot 6(H_2O)$	3	0.4 +/- 0.01	15	15
			2	8.6 +/- 0.03		
Contaminated 70% HTP / 30% TBP	Ce(+IV)	Cerium(IV) Ammonium Nitrate $(NH_4)_2Ce(NO_3)_6$	10	10 +/- 0.01	30	-
			10	10 +/- 0.01		
Contaminated 70% HTP / 30% TBP + Pure HNO_3 3M, Ratio 1:1	Ce(+IV)	$(NH_4)_2Ce(NO_3)_6$	10	10 +/- 0.01	15	15
			10	10 +/- 0.01		
Contaminated 70% HTP / 30% TBP	Ru(+III)	Ruthenium(III) Nitrosylnitrate $RuNO(NO_3)_3$	3	0.6 +/- 0.1	30	-
			3	0.6 +/- 0.1		
Contaminated 70% HTP / 30% TBP + Pure HNO_3 3M, Ratio 1:1	Ru(+III)	$RuNO(NO_3)_3$	3	0.6 +/- 0.1	15	15
			3	0.6 +/- 0.1		

189
190

191
192
193
194
195
196
197
198
199
200
201
202
203
204
205
206
207

II.B. Combustion test bench

Thermal degradation and ARF measurements were carried out on a specifically designed experimental test bench¹². Figure 1 summarizes the main schematic route of the thermal degradation and sampling devices. A ventilation fan coupled to a calibrated diaphragm allows for the injection of air at a fixed flow-rate (40 m³/h for the present study) inside the degradation chamber including a radiant conical heater (not used in the present study). Particles are then extracted from this chamber inside an exhaust duct heated at 150°C before being sampled under well-mixed conditions 2 meters downstream from the inlet. Finally, particles are trapped on HEPA filter (pleated glass fiber filter reference 1505.40.00 from CAMFIL[®]) before releasing exhaust gases in the atmosphere. As reported in bibliographical analysis presented in the introduction of the present article, most of experimental test benches previously used were not optimized to reduce particle losses by walls or ducts deposition. In most cases, a lack of knowledge on particle transfer function within the test bench may partially explain disparities in terms of ARF values reported between different studies even for a given fuel or similar experimental conditions. As a consequence, and to avoid such disparities, our test bench was optimized for reducing particles losses in the combustion chamber and the exhaust duct. In addition, transport efficiency measurements and computational fluid dynamics calculations (CFD) were carried out for a range of aerodynamic diameters in agreement with those associated to released particles (more details could be retrieved in¹²).



208
209
210

Figure 1: Diagram of the combustion test bench

211 A small part (reported as $P_{p(\%)}$ in this study and defined as the ratio between volumetric sampling flow rate and
212 exhaust flow rate) of the overall exhaust flow was sampled on HEPA membrane (Cellulose acetate, SARTORIS
213 11106-47-N, 47 mm diameter with 0.45 μm pore diameter) with an isokinetic probe. The mass of cerium or
214 ruthenium composing released particles sampled on membranes were then determined by ICP-MS/AES
215 (Inductively Coupled Plasma Mass Spectrometry/Atomic Emission Spectroscopy) or X-Ray Fluorescence
216 analyses, respectively.

217 Taking into account transport efficiency of particles in the combustion test bench and experimental sampling
218 conditions, the definition of the airborne release fraction is:

$$219 \quad \text{ARF} = \frac{m_{\text{element}}^{\text{sampling}}}{m_{\text{element}}^{\text{initial}} \cdot P_{p(\%)} \cdot F_{p(\%)}} \quad (\text{Eq. 2})$$

220
221 with:

- 222 • $m_{\text{element}}^{\text{sampling}}$ the mass of released element (Ce or Ru) determined on sampling the membrane,
- 223 • $m_{\text{element}}^{\text{initial}}$ the mass of element (Ce or Ru) initially diluted in the HTP/TBP solution,
- 224 • $P_{p(\%)}$ the ratio between volumetric sampling flow rate and exhaust flow rate,
- 225 • $F_{p(\%)}$ the penetration fraction of particles within the facility and depending on the aerodynamic diameter
226 of released particles.

227
228 For each element (Ce or Ru), it is then crucial, to compute the ARF, to determine the released aerosol size
229 distribution and its corresponding penetration factor within the test bench from the emission point to the sampling
230 point. As previously demonstrated ¹², particle losses in this test bench could be considered negligible for
231 aerodynamic diameter lower than 5 μm . In the present study, we will demonstrate that released particles are within
232 this lower size range and we will assume, for easing ARF computation, the penetration factor $F_{p(\%)}$ as equal to 1
233 (or 100%).

234 **II.C. Experimental protocol and analysis of samples**

237 Contaminated solutions are prepared a few minutes before combustion experiments since stability of
238 cerium or ruthenium within solvents could not be maintained for all conditions ³². A small amount of solvent is
239 then analysed by ICP-MS after the extraction protocol giving the initial concentration of the organic phase in terms
240 of contaminant. This concentration is of main importance since it gives the initial mass contaminant mass in the
241 liquid phase m_{initial} needed for computing ARF according to eq. 2.

242 Contaminated solvents are then placed in a cylindrical borosilicate glass container with an internal
243 diameter of 48 mm and a volume of 50 mL. 30 mL of contaminated HTP/TBP and 15 mL of contaminated
244 HTP/TBP + 15 mL HNO_3 3M are respectively considered for mono and biphasic experiments. Borosilicate glass
245 container is placed in the combustion chamber and ignited with a blowtorch during a short period (5 seconds) in
246 order to avoid Ce(+IV) reduction to Ce(+III) as previously reported ³². After ignition, extraction air flowrate (40
247 m^3/h) is applied in the combustion chamber and emitted particles (soot and released cerium or ruthenium
248 containing particles) are sampled on cellulose acetate membranes.

249 Special care was considered in quantification methods useful for measuring the mass of contaminant
250 released during experiments. For this purpose, two different approaches were considered; ICP-MS for cerium-
251 based particles and X-Ray Fluorescence for ruthenium-based particles.

252 Dealing with ICP-MS, key issue remains in digestion step and a specific calibration protocol was applied
253 in terms of yield in agreement with protocol previously validated by our team ¹². For cerium samples, acid digestion
254 has been considered for completing in an efficient way the dissolution of filters and sampled particles within a
255 liquid medium suitable for ICP-MS analysis. For calibrating the overall ICP-MS procedure, reference filters

256 containing a known amount of cerium oxide powder (5 μm CeO_2 powder, REacton®, 99.9% reference 215-150-4
 257 from Alfa Aesar) were prepared and analysed. For this purpose, cerium oxide powder was aerosolized using a
 258 vortex shaker unit and the deposited mass was determined by weighing the membrane before and after powder
 259 dispersion. The digestion yield of ICP-MS analysis, mainly associated to the process of dissolution or digestion of
 260 sample from solid to liquid phase, was then determined by comparing the mass of considered element obtained by
 261 ICP-MS with the mass deposited on the reference membrane. More details on the determination of the digestion
 262 yield are available in supplementary materials (SI-I). According to this protocol, the mass of particles composed
 263 by the element Ce and sampled on membranes during experiments is defined by:

264

$$265 \quad m_{\text{Ce}}^{\text{sample}} = \frac{m_{\text{Ce}}^{\text{ICP-MS}}}{Y_{\text{detection ICP-MS}}^{\text{chemical form of Ce}} \cdot Y_{\text{digestion}}^{\text{chemical form of Ce}}}, \quad (\text{Eq. 3})$$

266 with:

- 267 • $m_{\text{Ce}}^{\text{sample}}$: mass of element Ce sampled on membrane (kg),
- 268 • $m_{\text{Ce}}^{\text{ICP-MS}}$: mass of element Ce quantified by ICP-MS analysis (kg),
- 269 • $Y_{\text{detection ICP-MS}}^{\text{chemical form of Ce}}$: ICP-MS's yield of detection of element Ce,
- 270 • $Y_{\text{digestion}}^{\text{chemical form of Ce}}$: yield of digestion of element Ce in its chemical form as sampled on membrane, as
 271 determined according to the calibration protocol using reference membranes.

272 Similar qualification protocol was applied to ruthenium samples, using RuO_2 powder (micron size RuO_2
 273 powder, 99.9% reference A10816 from VWR). Nevertheless, we were not able to identify digestion protocol able
 274 to fully dissolve our reference samples and relevant for further ICP analysis. Direct analysis method by X-Ray
 275 fluorescence was then preferred to ICP-MS and was calibrated according to the same reference membranes. For
 276 this purpose, X-ray source (88 kV with a tungsten anode) and CdTe spectrometer (X-123 CdTe X-Ray
 277 spectrometer from Amptek) were mounted on an exposure cell devoted to the analysis of membrane samples. More
 278 details on this calibration are available in supplementary materials (SI-II). For this second analysis method, the
 279 mass of ruthenium associated to our samples are computed according to:

$$280 \quad m_{\text{Ru}}^{\text{sample}} = a \cdot m_{\text{Ru}}^{\text{XRF}} + b, \quad (\text{Eq. 4})$$

281 with:

- 282 • $m_{\text{Ru}}^{\text{sample}}$: mass of element Ru sampled on membrane (kg),
- 283 • $m_{\text{Ru}}^{\text{XRF}}$: intensity associated to the integral of the Ru peak recorded by XRF (count per second),
- 284 • a, b: calibration factors of XRF spectrometer (see SI-II).

285 In parallel to ARF determination, Scanning Electronic Analysis of membranes was also performed for
 286 determining elemental composition, morphology and size distribution of cerium and ruthenium released particles.
 287 Imaging was conducted using a JEOL Scanning Electron Microscope (SEM) JSM 6010-LV and a ZEISS SEM-
 288 FEG GEMINI associated to Energy-dispersive X-ray spectroscopy (EDS) for elemental composition analysis.
 289 Projected area equivalent diameters of the considered particles were then determined directly on SEM
 290 micrographs.

291

292 **III. Experimental results**

293

294 **III.A. Physico-chemical properties of released particles**

295

296 Analysis of 60 to 2000 particles was conducted for both contaminant (Ce or Ru). SEM illustrations of
 297 particles emitted from Ce(+III), Ce(+IV) and Ru(+III) contaminated solvents are presented in Table III. Circularity
 298 (defined as $4\pi \text{Area}/\text{Perimeter}^2$) of the particles was measured on each SEM image using the ImageJ software and
 299 orders of magnitude of this shape descriptor are presented in Table III. Size distribution properties and elemental

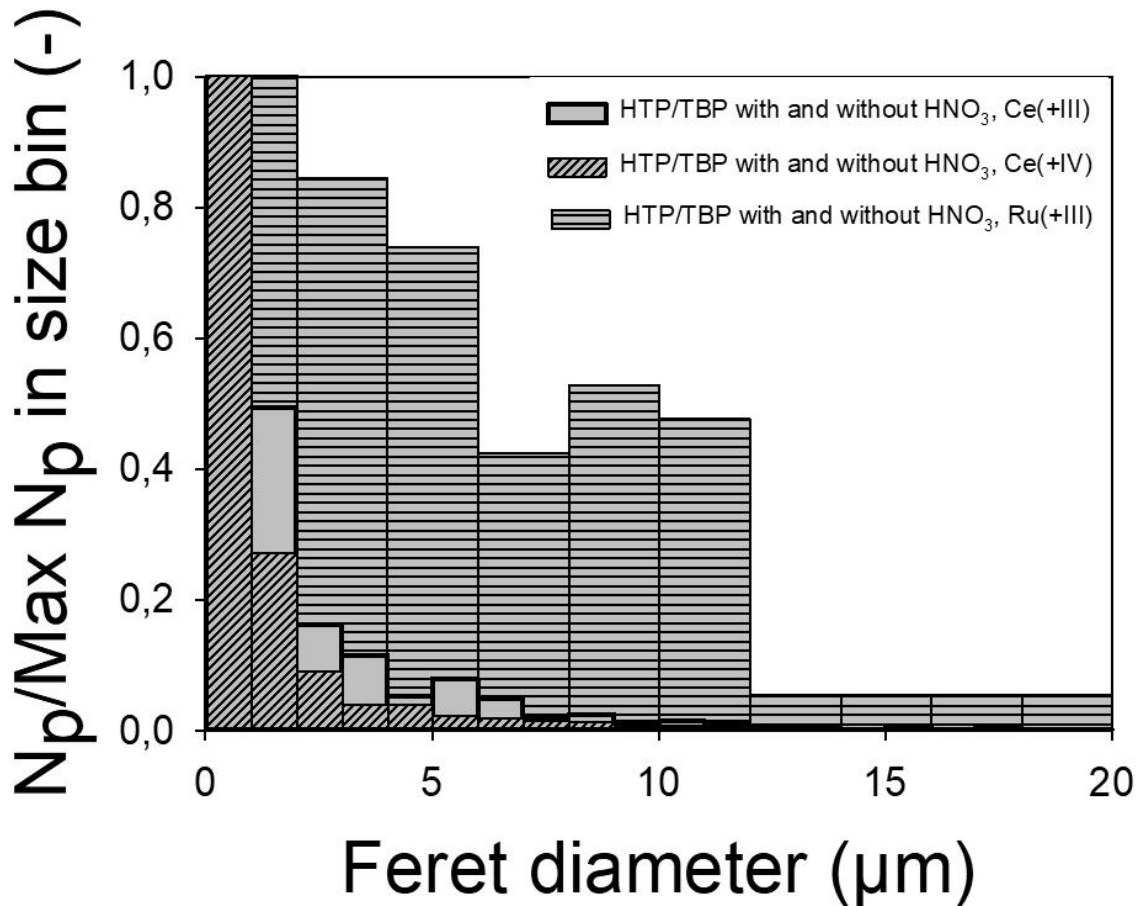
300 composition (performed by EDS analysis) are also presented in Table IV. Since a minimum number of particles is
301 required for both size and shape statistical analysis, respectively 550 and 100 particles⁴³, SEM pictures of particles
302 emitted from organics and organics/nitric solutions were merged and considered in the same data set for each
303 contaminant. One must notice that size analysis was limited to particle diameter larger than 0.2 μm considering
304 the SEM's resolution and corresponding Feret diameters (defined as the longest distance reported between any
305 two pixels composing the particle). These data are then reported in Table III.

306 Figure 2 exhibits the size distribution in terms of Feret diameter of particles emitted for Ce(+III), Ce(+IV)
307 and Ru(+III). Regarding particles shape, Table III presents illustrations of SEM images recorded for each
308 contaminant and fuel composition (with and without HNO_3). Since sampled particles could be characterized by a
309 wide range of elongated or complex morphology, we introduced a circularity threshold to quantify contribution of
310 "quasi perfect shape" spherical particles to other type of particles. For this purpose, a circularity criteria was fixed
311 at a threshold of 0.995 and corresponding fraction of particles presenting a circularity higher than this threshold
312 was computed. This threshold was determined according to a statistical analysis of 365 images of nearly perfect
313 spherical reference polystyrene latex and glass particles (geometric diameter ranging from 2.5 to 10 μm).

314 Dealing with ruthenium, particles emitted and released during the combustion of HTP/TBP solutions
315 contaminated by ruthenium nitrosyl nitrate are characterized by a wide range of particle morphology, composition
316 and size distribution. Regarding particle shape, less than 10 % of particles fulfilled the 0.995 criteria for particle
317 circularity, highlighting complex and variable particle shapes as it could be noticed on SEM images reported in
318 table III. For this contaminant, particles present bimodal size distribution for both mono and biphasic conditions.
319 Two peaks Gaussian fitting was applied to the size distribution obtained by merging mono and biphasic conditions,
320 and modal Feret diameters of 1 μm and 10 μm were reported. Notice that this complex size distribution supports
321 the hypothesis that airborne resuspension is due, for ruthenium, to two distinct mechanisms, bubble bursting and
322 volatility, potentially occurring at the same time and with a prevalence of volatility.

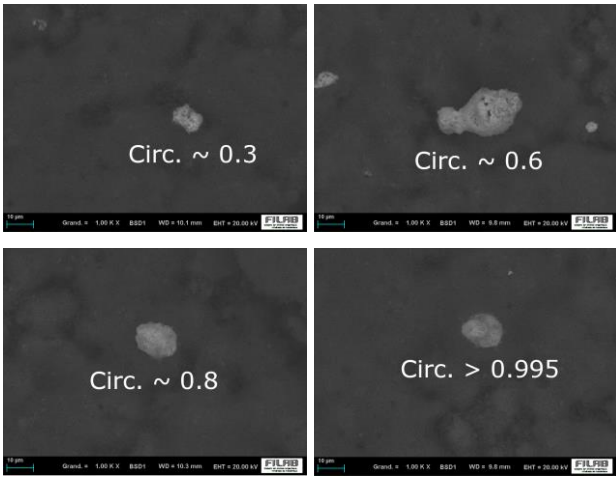
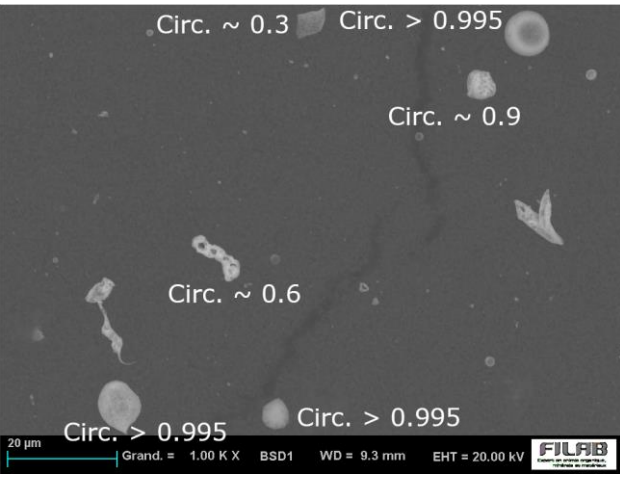
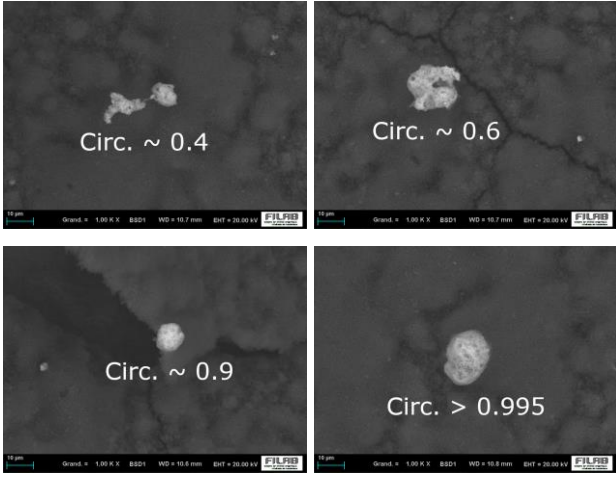
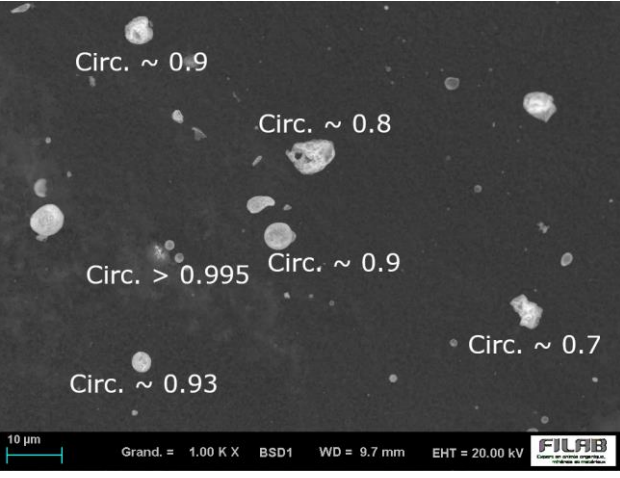
323 Concerning elemental composition of ruthenium particles, most of them are composed of pure ruthenium
324 (57-71 % of all analysed particles). Nevertheless, a significant contribution of phosphorous and phosphorous-
325 oxygen containing particles are also observed (11-13% and 17-32 %, respectively). As previously reported³⁹,
326 extracted ruthenium is present in the form of two main complexes in the organic phase ($(\text{TBP})_3\text{RuNO}(\text{NO}_3)_3(\text{H}_2\text{O})_2$
327 and $(\text{TBP})_2\text{RuNO}(\text{NO}_3)_3(\text{H}_2\text{O})_2$ with a predominance of the tris-TBP complex for $[\text{HNO}_3]$ concentration at 3 M).
328 Lefebvre et al.⁴⁴ also reported that nitrosyl form of ruthenium complexes was maintained in the organic phase
329 without TBP in the first coordination sphere of Ru, potentially linked through a water molecule. Furthermore,
330 thermal degradation of ruthenium nitrosyl is also known as a route to produce RuO_2 particles⁴⁵ under oxidative
331 conditions. In the present study, evidence of metallic form of ruthenium, as the major form of released particles,
332 supports the idea introduced by Bouilloux¹⁵, that reductive conditions are representative of those encountered
333 within studied TBP/HTP flames. Under such non-oxidative conditions, Duvigneaud & Reinhard-Derie⁴⁶ reported
334 emission of Ru(metal) and RuO_2 from the thermal decomposition of Ru(+III) hydrate. This abundance release of
335 Ru in metal form from the thermal degradation of Ru(+III) is in agreement with the presence of pure Ru particles
336 released under our present experimental conditions. Nevertheless, and as reported by Duvigneaud & Reinhard-
337 Derie⁴⁶, Ru(metal) is not expected to be the predominant chemical form of emitted ruthenium under non-oxidative
338 conditions. As mentioned by those authors⁴⁶, RuO_2 should be the most predominant ruthenium form, in strong
339 dis-agreement with the absence, under the present experimental conditions, of released particles solely made of
340 Ru and O in Table IV. To explain this discrepancy, one must keep in mind that in the present study, significant
341 quantities of organophosphates and phosphoric acid are available in liquid⁴⁷ or gas phases^{3,26}. Such abundance of
342 phosphorus in organic or acid forms react⁴⁸ or be strongly adsorbed⁴⁹ with RuO_2 to generate ruthenium
343 organophosphates (Ru, P, O) that could further be reduced to Ru, P. In addition to this major contribution of
344 ruthenium reactivity to the overall airborne release, bubble bursting release could be another mechanism for
345 explaining the significant contribution of ruthenium organophosphates in the aerosol phase, as reported hereafter
346 for the cerium contaminant. Nevertheless, further analysis are needed (as an example particle analysis by Raman
347 spectroscopy) to confirm the chemical nature of particles made of Ru, P and O.

348 Considering cerium contaminated solvents, contribution of quasi perfect spherical particles (circularity
 349 higher than 0.995) reaches 40 % and 58 % for Ce(+III) and Ce(+IV), respectively. This huge contribution of
 350 spherical particles supports the assumption of airborne release mainly driven by bubble bursting and rapid droplet
 351 drying in the flame ^{38,50,51} leading to the formation of dry particles containing the contaminant element, in close
 352 agreement with recent findings ²². Size distributions reported in Figure 2 show major distribution of particles with
 353 a Feret diameter lower than 5 μm with a count median diameter (determined by log-normal fitting on the size
 354 distribution obtained by merging Ce(+III) and Ce(+IV)) of 0.8 μm and a geometric standard deviation of 2.9.
 355 These results are in good agreement with the “sphere like” shape particles with an optical diameter of nearly 1-2
 356 μm previously reported for uranium contaminated kerosene-TBP solutions ¹⁴ and more recently for lanthanides
 357 nitrates (Lu, Yb and depleted uranium ²²). Under all our experimental conditions, released particles are composed
 358 of cerium, phosphorus and oxygen. Due to the presence of soot in analysed samples, mainly composed of carbon,
 359 phosphorus and oxygen ³, we were not able to conduct a stoichiometric analysis of the elemental composition of
 360 cerium based particles. Nevertheless, the homogeneous composition of cerium-based released particles supports
 361 the assumption that they are mainly in the form of the most thermally stable cerium phosphate CePO_4 ^{52,53} in
 362 agreement with lutetium and ytterbium phosphates reported by Hubbard et al. ²², highlighting a potential reduction
 363 of Ce(+IV) into Ce(+III) during their airborne release.



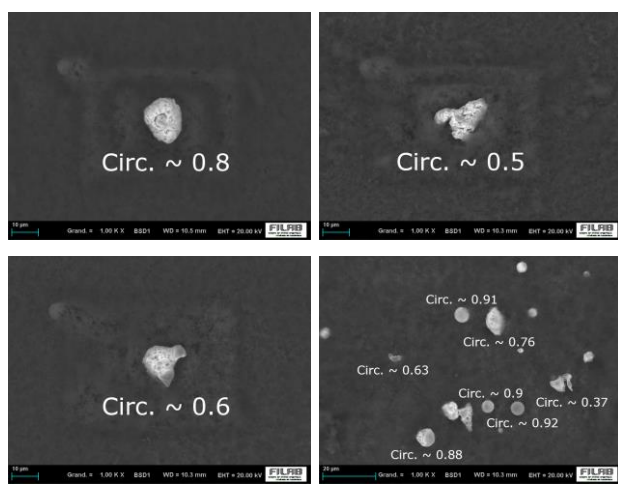
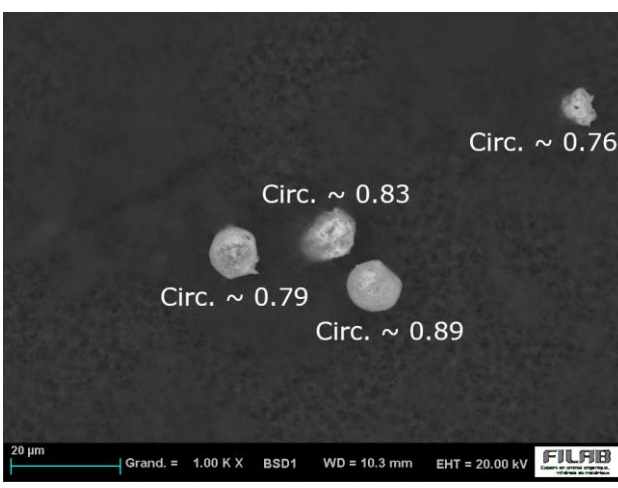
364 Figure 2: size distributions of particles released during combustion of contaminated organics with and without
 365 HNO_3 at 3M
 366
 367

368 Table III - part 1: Scanning Electronic Microscopy images of released particles from cerium contaminated solutions

Fuel composition → Contaminant ↓	Contaminated organics 70% HTP / 30% TBP	Contaminated organics 70% HTP / 30% TBP Pure HNO ₃ 3M, Ratio 1:1
Ce(+III) 10 g Ce/L		
Ce(+IV) 10 g Ce/L		

369

370 Table III - part 2: Scanning Electronic Microscopy images of released particles from ruthenium contaminated solutions

Fuel composition → Contaminant ↓	Contaminated organics 70% HTP / 30% TBP	Contaminated organics 70% HTP / 30% TBP Pure HNO ₃ 3M, Ratio 1:1
Ru(+III) 0.6 g Ru/L		

371
372
373
374
375
376
377
378
379
380
381

382 Table IV: elemental composition and size properties of released particles

Fuel composition (in volume)	Contaminant	Number of particles	Composition by EDS analysis	Min-Max projected diameters (μm)	Overall size distribution
Contaminated 70% HTP / 30% TBP	Ce(+III) at 10 g Ce/L	59	100% with Ce, O, P	-	CMD = 0.8 μm $\sigma_g = 2.9$
Contaminated 70% HTP / 30% TBP + Pure HNO ₃ 3M, Ratio 1:1	Ce(+III) at 10 g Ce/L	1109		1 – 6 μm	
Contaminated 70% HTP / 30% TBP	Ce(+IV) at 10 g Ce/L	114		3 – 4 μm	
Contaminated 70% HTP / 30% TBP + Pure HNO ₃ 3M, Ratio 1:1	Ce(+IV) at 10 g Ce/L	2191		1 – 5 μm	
Contaminated 70% HTP / 30% TBP	Ru(+III) at 0.6 g Ru/L	237	71% pure Ru 17% Ru, O, P 13% Ru, P	1 – 23 μm 1 – 12 μm 7 – 17 μm	Two peaks Gaussian fit Mode 1: 1.0 μm Mode 2: 10 μm
Contaminated 70% HTP / 30% TBP + Pure HNO ₃ 3M, Ratio 1:1	Ru(+III) at 0.6 g Ru/L	92	57% pure Ru 32% Ru, O, P 11% Ru, P	1 – 14 μm 1 – 36 μm 3 – 28 μm	

383

III.B. Airborne release fractions

A set of 9 different experimental conditions were considered with at least 2 repetitions each. Corresponding values are reported in Tables SI-I to SI-III in Supplementary Information with corresponding experimental uncertainties. Mean values associated to each experimental condition are summarized in Table V including absolute uncertainties (within 95% confidence interval) computed by taking into account the absolute experimental uncertainties (see SI-3 for more detail) of each ARF and the standard deviation determined from the entire set of ARF reported for this condition.

Considering solutions contaminated with cerium at nearly 10 g/L (bold values in Table V), ARF mean values appear to be similar despite the oxidation state of cerium. Mean values of 0.22 % +/- 0.31 % and 0.20 % +/- 0.28 % are then reported for monophasic Ce(+III) and Ce(+IV) contaminated organic solutions, respectively. These results are in agreement, within the confidence interval, with values previously reported^{16,23} for small scale experiments. Contribution of non-contaminated aqueous phase to ARF also appears significant with values 5 to 8 times higher for biphasic experimental conditions (1.78 % +/- 1.06 % and 1.01 % +/- 1.31 % for Ce(+III) and Ce(+IV), respectively). This promoting influence of aqueous phase confirms that resuspension is mainly driven by pool boiling and bubbles bursting as previously mentioned in the literature^{15,36} and discussed in the present study. Beyond the contribution of aqueous phase to ARF, experiments were also conducted for Ce(+III) at several contamination levels (from 0.2 to 9.3 g/L of Ce(+III)). Nevertheless, extended uncertainties do not allow us to clearly identify a significant trend of ARF as a function of Ce concentration.

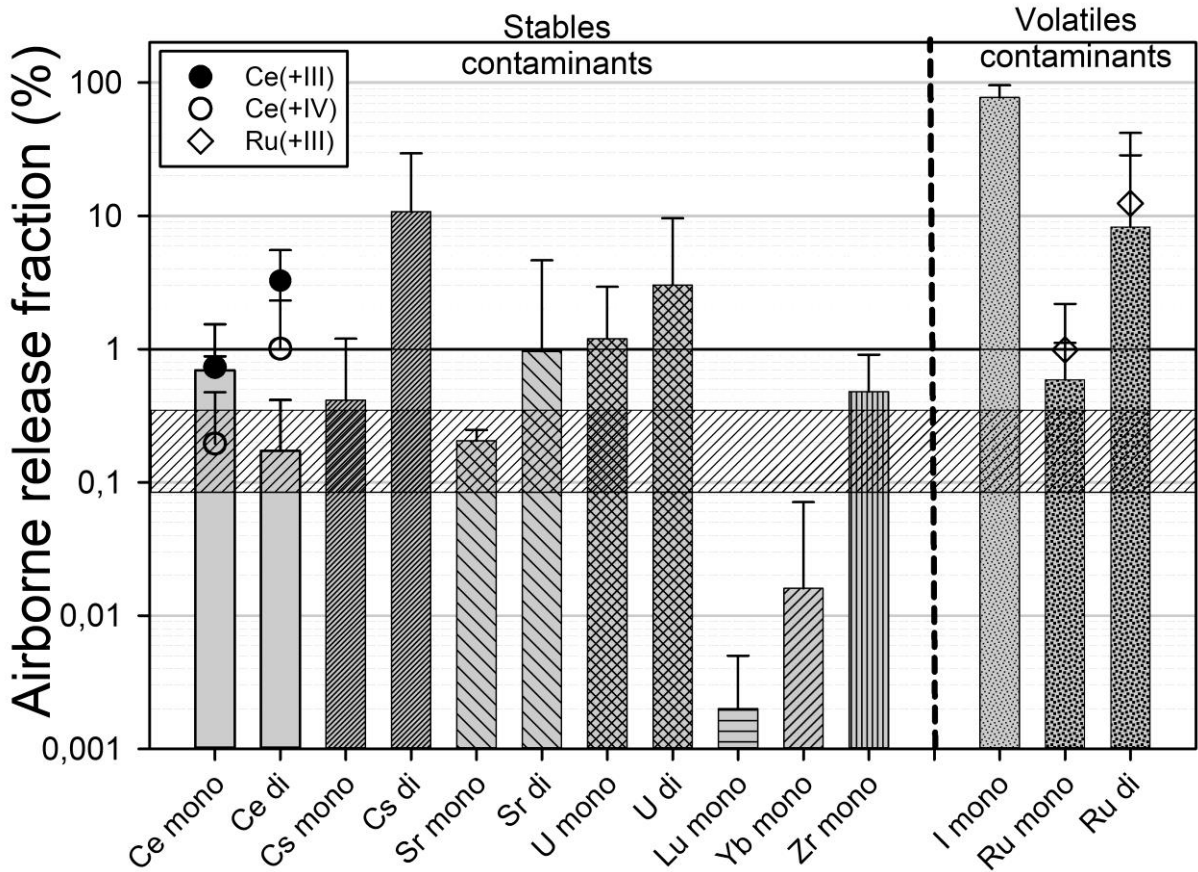
Regarding ruthenium Ru(+III) contaminated solutions, ARF appears significantly higher even for solutions contaminated at a lower level (0.6 g/L). Furthermore, high level of uncertainty is reported for biphasic conditions, supporting the volatile nature of ruthenium released suspected to be highly influenced by sampling conditions and potentially explaining this large level of experimental dispersion (see SI-3 for ARF values reported for each experimental repetitions).

Table V: mean Airborne Release Fractions (ARF) determined for each experimental condition (in bold, experiments conducted for surrogate concentrations close to 10 g/L)

Fuel composition (in volume)	Contaminant	Salt	[Cont _{org}] (g/L)	Mean ARF (%, extended uncertainty)
Contaminated 70% HTP / 30% TBP	Ce(+III)	Cerium(III) nitrate hexahydrate Ce(NO ₃) ₃ .6(H ₂ O)	0.2	0.58 % +/- 0.62 %
			4.8	1.56 % +/- 1.57 %
			9.3	0.22 % +/- 0.31 %
Contaminated 70% HTP / 30% TBP + Pure HNO ₃ 3M, Ratio 1:1			0.4	4.24 % +/- 2.12 %
			8.6	1.78 % +/- 1.06 %
Contaminated 70% HTP / 30% TBP	Ce(+IV)	Cerium(IV) Ammonium Nitrate (NH ₄) ₂ Ce(NO ₃) ₆	10	0.20 % +/- 0.28 %
Contaminated 70% HTP / 30% TBP + Pure HNO ₃ 3M, Ratio 1:1			10	1.01 % +/- 1.31 %
Contaminated 70% HTP / 30% TBP	Ru(+III)	Ruthenium(III) Nitrosylnitrate RuNO(NO ₃) ₃	0.6	0.99 % +/- 1.20 %
Contaminated 70% HTP / 30% TBP + Pure HNO ₃ 3M, Ratio 1:1			0.6	12.41 % +/- 29.45 %

A comparison of present results with values reported in the literature, summarized in Table I, is proposed in Figure 3. Present experimental results appear in agreement with previously reported values both for cerium and ruthenium contaminated HTP/TBP. Since we were not able to identify from the literature the experimental ARF values obtained for plutonium contaminated HTP/TBP, we also reported in Figure 3, through a dashed horizontal area, the range of ARF (from 0.0885 to 0.309 %) proposed by Ballinger et al.²⁴ from the FIRIN compartment fire code

418 for large scale solvent extraction fire including Pu(+IV) in the organic phase. It is worth noting that results obtained
 419 for Ce(+IV) for monophasic condition are within the range of ARF introduced by Ballinger et al. (1985) for Pu.
 420 Furthermore, values obtained for cerium in the present study appear in good agreement with mean values
 421 determined for uranium, a contaminant generally considered as a surrogate of plutonium release in case of fires
 422 involving fuels representative of the PUREX process. These conclusions support our main assumption that release
 423 of stable contaminants is mainly driven by bubble bursting and that the chemical nature of the contaminants (Ce,
 424 Cs, Sr, Zr and U) does not induce significant discrepancy in terms of ARF.



425
 426 Figure 3: Comparison of results obtained in the present study (circular and diamond dots) with mean values
 427 determined from values reported in the literature (from raw data extracted from each reference cited in Table I).
 428 Volatile and stable contaminants are considered separately. Dashed horizontal bar corresponds to the range of
 429 ARF associated to release of Pu as computed by Ballinger et al. ²⁴

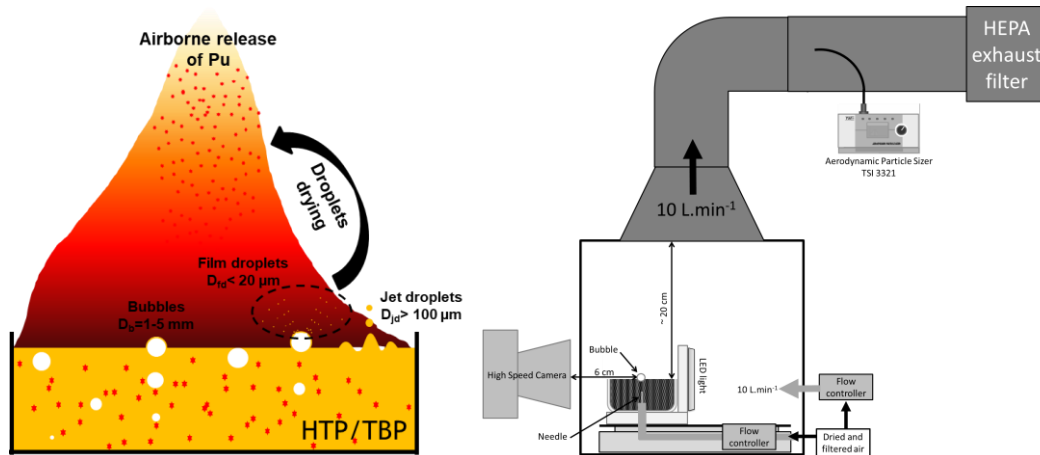
430 III.C. Phenomenological description

431
 432 As demonstrated both by SEM analysis of cerium released particles and comparison of ARF measured for mono
 433 and biphasic experimental configurations, bubble bursting is one of the main driven mechanism associated to
 434 airborne release during contaminated liquid fuels fires. To go further on the theoretical description of this
 435 mechanism, additional experiments were carried out firstly, to describe the size of bubbles formed in the organic
 436 phase prior to bursting and secondly, to mimic bubble bursting under non-flaming conditions for analyzing number
 437 and size of droplets finally formed. Figure 4 illustrates a simple phenomenological description of the contribution
 438 of bubble bursting to the release of particles during complex pool fires. As reported by several authors, airborne
 439 release associated to bubble bursting of aqueous salt solutions representative of seawater ⁵⁴⁻⁵⁶ or radionuclides
 440 contaminated water pool ^{38,57} mainly occurs through the formation of two different types of droplets. The first
 441 droplet emission process, mostly concerning small bubbles, is due to the breakage of the bubble cap, followed by
 442 a sudden pressure drop. In this case, a jet is formed and droplets are emitted from the fragmentation of this jet. The
 443 number N_{jd} and diameter D_{jd} of these droplets, named in the rest of this discussion as “jet droplet”, are inversely
 444 proportional to the bubble diameter as pressure drop is expected to be higher for smaller bubbles. Diameter of
 445 these droplets is generally one-tenth of the bubble diameter for seawater ⁵⁸. The second emission process identified
 446 during bubble bursting is associated to droplets emitted from the rupture of the liquid film forming the interface
 447 between the bubble cavity and the atmosphere. This release phenomenon is expected to be more efficient for
 448 millimetric bubbles ⁵⁴ with increasing number of “film droplets” per bubbles with increasing bubble diameter ⁵⁵.
 449

450 The diameter D_{fd} of these droplets is reported to linearly increase with bubble diameter with an average diameter
 451 of nearly 30-40 μm for bubble diameter in the range 2-3 mm for seawater^{56,59}. At the final stage of the release
 452 process, dry residues are emitted as solid particles and are defined, in terms of diameter $D_{geo, p}$, according to the
 453 following relationship:
 454

$$D_{geo, p} = D_d \sqrt[3]{\frac{C_m}{\rho_p}}, \quad (\text{Eq. 5})$$

455 with D_d the droplet diameter (m), C_m the mass concentration ($\text{kg}\cdot\text{m}^{-3}$) and ρ_p the dry particles density ($\text{kg}\cdot\text{m}^{-3}$).
 456
 457
 458

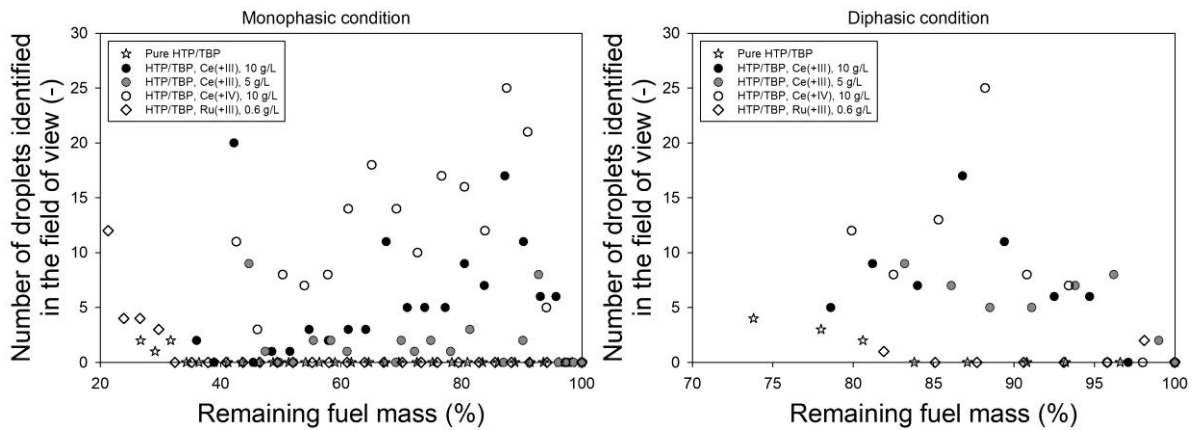


459
 460
 461 Figure 4: (left) phenomenological description of Pu particle released from bubble bursting during HTP/TBP pool
 462 fire, (right) diagram of the facility used for the study of the bubble and jet/film droplets formation under non-
 463 flaming condition
 464

465 Beyond these numerous studies available for release and formation of salt particles from boiling or bursting water
 466 contaminated solutions, as far as we are concerned, no experimental study is available regarding the properties of
 467 bubbles and droplets formed during HTP/TBP combustion. To fill this lack of knowledge, and to bring
 468 experimental analysis of bubbles and droplets emissions fundamental for simulation of contaminant release from
 469 liquid fuel fire, the present study aims to characterize all these phenomena under as much representative conditions
 470 as possible.

471 For this purpose, and to measure the size and number of bubbles emitted as a function of time for pure and Ce(+III),
 472 Ce(+IV) or Ru(+III) contaminated HTP/TBP under mono or biphasic conditions, bubble bursting was
 473 characterized using a High-Definition (HD) camera (SONY HDR-SR11) placed at 90° of the cylindrical
 474 borosilicate glass container of the test bench. The optical focusing was carried out at the centre of the sample
 475 holder with a corresponding field of view covering the entire diameter of the glass container. Optical depth of field
 476 and focusing were fixed constant over the test in order to avoid any misinterpretation of millimetric bubble
 477 diameter potentially present above or beyond the observation area. Scale was determined using a 30 mm ruler and
 478 corresponding size resolution was of 30 μm per pixel. Images recorded by HD camera were analyzed during 25
 479 minutes after the ignition with a time period of 1 minute. Figure 5 presents the evolution of number and diameter
 480 of droplets determined on each picture for monophasic (left part of Figure 5) and biphasic conditions (right part of
 481 Figure 5) as a function of remaining mass of fuel. For pure and Ru(+III) contaminated solutions, no bubble was
 482 reported during the major part of the experiments. This limited formation of bubbles during fire test could be
 483 explained by limited abundance of “bubbles nuclei” within HTP/TBP for pure and low Ru(+III) contaminated
 484 solutions (0.6 g/L). On the other hand, the slight increase of emission identified at the end of fire tests, at nearly
 485 30 % of remaining fuel mass for monophasic condition is due to the formation of residues within pure solvent and
 486 increase of Ru(+III) concentration within the residual solvent since major part of Ru(+III) still remains in the
 487 organic phase (with relatively low ARF values reported in Table V). The low ability of Ru(+III) contaminated
 488 solutions to produce bubbles prior to TBP combustion and formation of residues supports our previous assumption
 489 that the ruthenium release is mainly ruled by its volatility rather than bubble bursting.

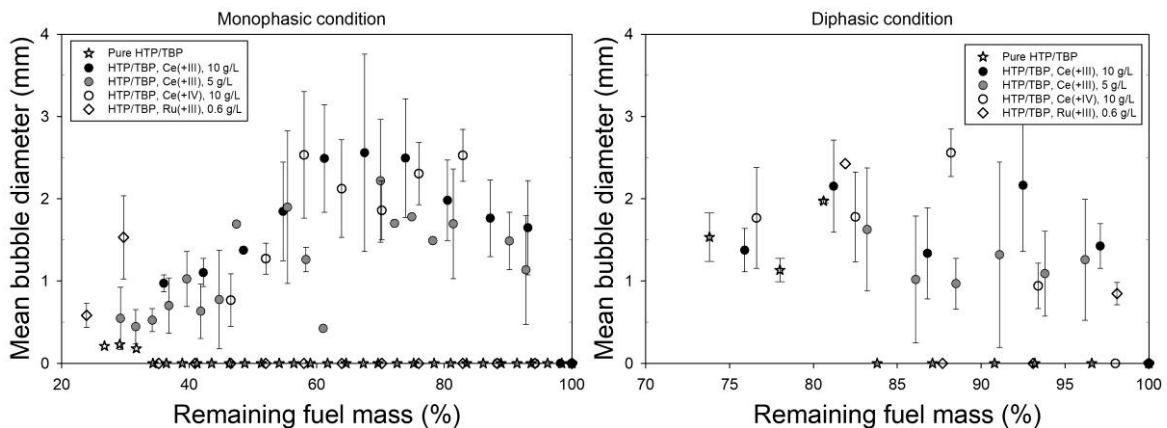
490 Regarding Ce(+III) and Ce(+IV) contaminated solutions at 10 g Ce/L, continuous emission of bubbles could be
 491 noticed in Figure 5 with similar level of emission between both cerium oxidation state. Unlike the case of
 492 ruthenium, comparison of results reported for lower contamination level (5 g Ce/L) for Ce(+III) does not allow to
 493 draw any conclusion on the influence of concentration in the range 5 - 10 g/L. Consequently, the threshold
 494 concentration of “bubbles nuclei” to reach continuous emission of bubbles must be in the range 0.6 - 5 g/L.



495
496
497
498
499
500
501
502
503
504
505
506
507
508

Figure 5: Evolution, as a function of remaining fuel (HTP/TBP) mass, of number of bubbles formed at the liquid interface during fire experiments of (left) HTP/TBP monophasic pool fire and (right) biphasic HTP/TBP – 3M HNO₃ pool, both containing different cationic species (Ce(+III), Ce(+IV), Ru(+III)).

Figure 6 presents the evolution of mean diameter of bubbles as a function of time since ignition. In agreement with the evolution of number of bubbles, mean diameters reported for pure and Ru(+III) contaminated solvents confirm limited emission of bubbles for these solutions and for both mono and biphasic conditions. For solvents contaminated by cerium, mean bubble diameters are mostly ranging between 1 and 3 mm for both mono and biphasic conditions. Evolution of mean bubble diameter as a function of time appears more pronounced for monophasic with an increase of diameter from 90 % to 60 % of remaining fuel mass followed by a constant decrease of mean bubble diameter until flame extinction.



509
510
511
512
513
514
515
516
517
518
519
520
521
522
523
524
525
526
527
528

Figure 6: Evolution, as a function of remaining fuel (HTP/TBP) mass, of mean bubble diameter at the liquid interface during fire experiments of (left) HTP/TBP monophasic pool fire and (right) biphasic HTP/TBP – 3M HNO₃ pool, both containing different cationic species (Ce(+III), Ce(+IV), Ru(+III)).

In a second time, this investigation of bubble diameter formed during HTP/TBP pool (containing different cationic species (Ce(+III), Ce(+IV), Ru(+III)) fire was considered to mimic synthetic bubbles under non-flaming conditions. This non-flaming study was carried out in order to analyse the number and the diameter of jet and film droplets formed during collapse of solvent bubbles. This experimental study does not aim to be fully representative of airborne release conditions (evolution of physical properties of solvent, drying/evaporating conditions) during HTP/TBP combustion but only to focus on the formation of droplet through bubble bursting and to demonstrate that this mechanism is the main driving force. For this purpose, an experimental test bench was designed as shown in Figure 4. Bubbles were formed in a square glass container presenting a glass tube in its centre for injecting dry and filtered pressurized air through needles with varying diameter. Experiments were conducted for pure HTP/TPB and contaminated HTP/TBP and in a range of bubbles diameter of 1 to 4 mm and jet droplets were identified and characterized using a High Speed Camera (NAC Hi-Dcam II).

Figure 7 presents the evolution of mean diameter and number of jet droplets emitted per bubble as a function of bubble mean diameter. Error bars correspond to standard deviation (k=1) associated to mean values reported in this figure.

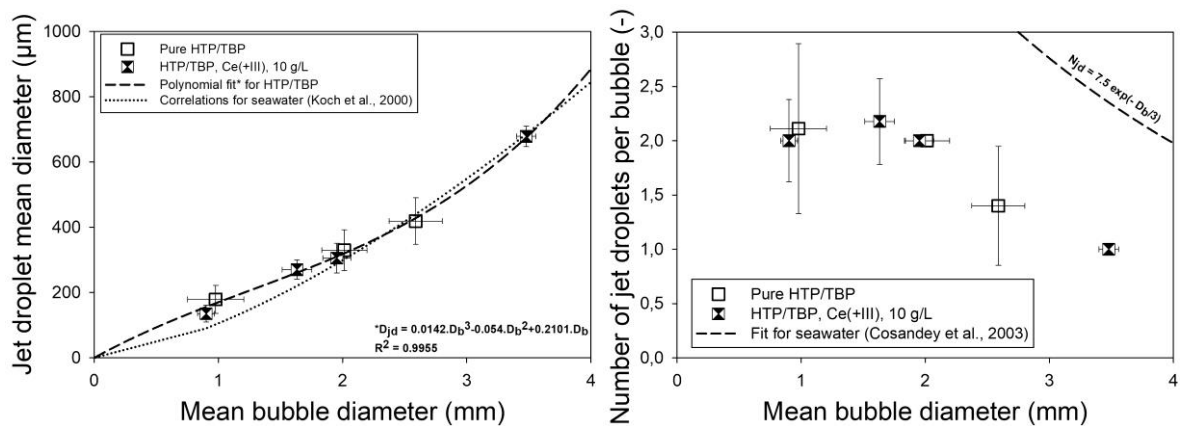


Figure 7: Evolution of mean jet droplet (left) diameter and (right) number emitted per bubble as a function mean bubble diameter

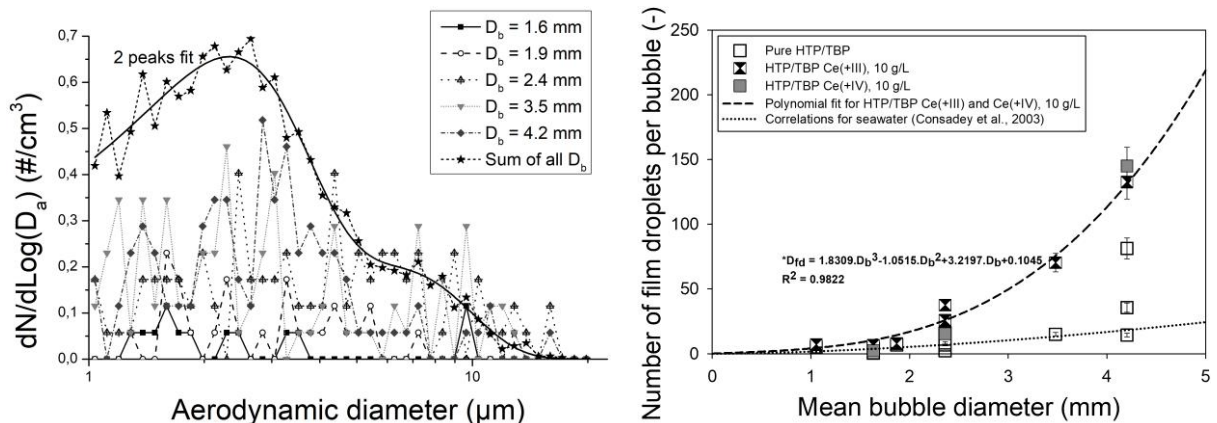
Considering jet droplet diameter, as reported in the literature^{38,57}, mean diameters are within 200-800 µm and appear to increase with increasing bubble size. Correlations proposed by Koch et al.⁵⁷ for seawater is in good agreement with present results, especially for bubble diameters larger than 2 mm. Nevertheless, since seawater and TBP/HTP present different physico-chemical properties, we propose a new empirical correlation for the entire range of bubble diameters. Corresponding third order polynomial fit appears in good agreement with both HTP/TBP measurements. A close agreement is also reported between pure and contaminated solvents, highlighting that present contamination level (10 g/L of Ce(+III)) and nature of this contaminant does not influence the fragmentation process. Considering the dimensionless approach proposed by Russel & Singh⁶⁰ and based on the Bond-Eötvös number describing the balance between gravitational forces compared to surface tension forces, this poor influence of Ce(+III) concentration is potentially due to a limited evolution of density and surface tension of contaminated solvents.

Regarding the number of jet droplets emitted per bubble (right part of Figure 7), a peak of emission is identified for bubble diameters in the range of those experimentally reported for flaming conditions (1 - 3 mm). This peak of release does not agree with the empirical evolution reported by Cosandey et al.³⁸ for seawater based on a relatively limited number of experimental values. On the other hand, a close agreement could be identified with results obtained by Blanchard & Syzdek⁵⁴ for seawater with a peak of emission of jet droplets for a bubble diameter close to 2 mm. Beyond the dispersion of results reported in the literature for different experimental set-up and conditions, present results obtained for HTP/TBP confirm that the release of jet droplet is limited to less than 3 droplets per bubble and that 400 µm diameter droplets emitted from 2 mm bubbles will be hardly transported in the aerosol phase. This is an additional demonstration that jet droplet may not fully explain the overall airborne release of particles from the contaminated liquid pool fire.

Additional measurements were then carried out to describe the emission of droplets through film breakage. For this purpose, an aerodynamic particle sizer (TSI APS 3321) was used to determine number concentration of dry particles formed according to the evaporation of film droplets and expected to present diameters lower than 20 µm⁵⁶. Dry and filtered air was injected in the test chamber and film droplets were transported from the emission point to sampling probe connected to the APS.

Left part of Figure 8 presents the size distributions of particles emitted for each mean bubble diameter (from 1.6 to 4.2 mm) over 3 hours of continuous bubbles bursting. As shown in Figure 8, the corresponding size distributions suffer from a lack of statistic and we were not able to propose any statistical analysis for each bubble diameter. Nevertheless, all experimental results were merged in order to build a mean size distribution (star symbols in Figure 8) of particles emitted during the bursting of bubbles presenting diameters from 1.6 mm to 4.2 mm. Two peaks Gaussian fitting procedures were applied (Origin Pro 8.6) to this mean size distribution and corresponding count modal aerodynamic diameter were respectively of 2.2 +/- 0.1 µm and 6.0 +/- 1.4 µm. This bi-modal size distribution confirms the influence of bubble diameter on the size of particles emitted⁶¹ with largest particle diameters associated to the larger bubbles. It is worth noting that corresponding count modal diameters could not be fully considered as the film droplets diameter since we were not able to avoid evaporation of these droplets and particle emission was recorded even for pure HTP/TBP. In the present situation, we could only suppose that film droplets may present diameter in a size range defined by the diameter associated to dry residue formed through droplet evaporation, and film droplet diameter which could be computed from this dry residue diameter. Assuming a spherical dry particle residue mainly composed of CePO₄ ($\rho_p = 5220 \text{ kg/m}^3$,³²), the diameter of the film droplet emitted from a solution contaminated at 10 g Ce/L could be computed from equation 5. The geometric diameter $D_{geo,p}$ in equation 5 is computed from count modal particles aerodynamic diameter $D_{a,p}$, determined in Figure 8,

576 and converted to geometric diameter $D_{geo,p}$ according to $D_{a,p} = D_{geo,p} \sqrt{\rho_p / \rho_0}$ (assuming spherical shape and
577 reference density ρ_0 of 1000 kg/m^3). According to equation 5, geometric diameters of film droplets are expected
578 to range between $6.5 \text{ }\mu\text{m}$ and $17.5 \text{ }\mu\text{m}$, in agreement with values commonly considered in previous studies ^{15,36}
579 from experimental measurements mainly carried out by Borkowski et al. ⁶². Comparison of aerodynamic diameter
580 of particles released from non-flaming bubble bursting (Figure 9) and from contaminated HTP/TBP pool fires (see
581 part III.a) shows again a good agreement. Assuming that particles released during flaming conditions are mainly
582 composed of monazite (CePO_4), count median geometric diameter reported in Table III could be converted to
583 aerodynamic diameter of $1.9 \text{ }\mu\text{m}$, in close agreement with values determined under non-flaming conditions.
584 Right part of Figure 8 presents the evolution of number of film droplets emitted per bubble as a function of mean
585 bubble diameter. For pure HTP/TBP, number of film droplets is not equal to zero, highlighting that film droplets
586 are not fully evaporated at the sampling point. Surprisingly, a good agreement is noticed between correlation
587 proposed by Cosandey et al. ³⁸ for seawater and pure HTP/TBP. On the other hand, bubbles produced by
588 contaminated solvents appear more efficient to release film droplets than seawater. This higher tendency of
589 solvents to release more droplets than water could be mainly explained by lower surface tensions reported for
590 kerosene/TBP or HTP/TBP mixtures ^{15,63}, close to 25 mN/m compared to seawater surface tensions of nearly 72
591 mN/m ⁶⁰. As recently observed experimentally ⁶¹, bubbles formed from lowest surface tension liquids produced
592 more particles with larger diameters. For predictive purpose, the evolution of the number of film droplets per
593 bubble could be correlated with the mean bubble diameter from a third order polynomial fit (see Figure 8). In the
594 range of bubble diameter reported under flaming conditions ($1\text{-}3 \text{ mm}$), the number of film droplets per bubble is
595 reported between 10 and 50, in reasonable agreement with the value of 10 particles emitted per 5 mm seawater
596 bubbles reported by Ke et al. ⁶¹. This larger amount of film droplets emitted per bubbles in comparison with jet
597 droplets confirms our first assumption, based on SEM analysis of released particles that ARF is mainly due to film
598 droplets rather than jet ones. Despite the mass balance in favour of jet contaminated droplets, it is worth noting
599 that such large droplets (from 200 to $800 \text{ }\mu\text{m}$) could not be transported by the convective flux of the pool fire flame
600 and are too influenced by the gravity and subject to settling (settling velocity ranging from 0.7 to 3 m/s ⁶⁴ for 200
601 $\text{-}800 \text{ }\mu\text{m}$ HTP/TBP droplets with a density of 827 kg/m^3 under ambient conditions ¹⁵), to be finally released in the
602 aerosol phase.
603



604
605 Figure 8: (left) mean film droplets size distribution formed during bursting of bubbles with different diameters
606 within HTP/TBP contaminated at 10 g Ce(+III)/L and (right) evolution of the number of film droplets emitted
607 per bubble as a function of mean bubble diameter
608

609 IV. Conclusions

610
611 The aim of this study was to enhance our state of knowledge on airborne release during contaminated pool fires
612 from a phenomenological point of view. For this purpose, experiments were conducted for three different
613 contaminants, cerium in two state of oxidation states (Ce(+III) and Ce(+IV)) and ruthenium (Ru(+III)). The
614 observed Airborne Release Fractions confirm the significant contribution of bubble bursting involved during
615 organic and aqueous boiling and for solutions contaminated by cerium in both oxidation states. ARF reported for
616 cerium are in good agreement with values previously determined, demonstrating a limited influence of the nature
617 of thermally stable contaminant (within the range of experimental uncertainty) on the final ARF and highlighting
618 the contribution of bubble bursting to the release phenomenon. On the other hand, higher ARF values reported for
619 ruthenium could only be explained by the volatility of chemical forms of this element emitted during HTP/TBP
620 pool fires.

621 To support these assumptions, scanning electronic microscopy analysis of released particles was performed. This
622 analysis has shown homogeneous composition and shape of particles emitted during combustion of cerium
623 contaminated solutions. On the other hand, wide variety of chemical composition and shape of ruthenium particles
624 confirms the volatile origin of these particles suspected to explain higher ARF values obtained for this element.
625 Additional analysis of size and number of bubbles produced during contaminated pool fires was conducted and
626 has confirmed, for pure or poorly contaminated organic solutions (Ru(+III) et 0.6 g/L), a limited formation of
627 bubbles. Considering highest level of contamination (from 5 to 10 g/L of cerium), significant emission of 1-3 mm
628 bubbles was reported. This bubble characterization, conducted under fire conditions, was used to conduct non-
629 flaming experiments to describe for the first time jet and film droplets emitted for different HTP/TBP bubbles
630 diameters. Jet droplets diameters, in the range 200 – 800 μm and number of film droplets (less than 20 μm in terms
631 of diameter) emitted per bubbles are closely linked to bubble diameter. Empirical correlations were proposed for
632 predictive purpose. Finally, a good agreement was demonstrated between diameters of particles released during
633 pool fire of cerium contaminated solvents and particles produced during drying/evaporation of film droplets
634 emitted during non-flaming bubble bursting experiments. This result finally confirms that bubble bursting is the
635 main driving mechanism explaining the airborne release of non-volatile contaminant during this type of hazardous
636 scenario.

- 638 1. R. S. HERBST, P. BARON, and M. NILSSON, *Standard and advanced separation: PUREX processes*
639 *for nuclear fuel reprocessing*, in *Advanced Separation Techniques for Nuclear Fuel Reprocessing and*
640 *Radioactive Waste Treatment*, Woodhead Publishing Limited (2011);
641 <https://doi.org/10.1533/9780857092274.2.141>.
- 642 2. B. NAJAFI et al., “History of Fire Events in the U.S. Commercial Nuclear Industry,” in 10th
643 International Conference on Nuclear Engineering, Volume 2, pp. 381–388, ASMEDC (2002);
644 <https://doi.org/10.1115/ICONE10-22587>.
- 645 3. F.-X. OUF et al., “Physicochemical properties of aerosol released in the case of a fire involving
646 materials used in the nuclear industry,” *J. Hazard. Mater.* **283**, 340 (2015);
647 <https://doi.org/10.1016/j.jhazmat.2014.09.043>.
- 648 4. T. HERTZBERG and P. BLOMQUIST, “Particles from fires - A screening of common materials found
649 in buildings,” *Fire Mater.* **27** 6, 295 (2003); <https://doi.org/10.1002/fam.837>.
- 650 5. J. FLOYD, O. K., and E. O., “Soot Deposition and Gravitational Settling Modeling and the Impact of
651 Particle Size and Agglomeration,” *Fire Saf. Sci.* **11**, 174 (2014).
- 652 6. E. BRUGIÈRE et al., “Increase in thermophoretic velocity of carbon aggregates as a function of particle
653 size,” *J. Aerosol Sci.* **76**, 87 (2014); <https://doi.org/10.1016/j.jaerosci.2014.06.007>.
- 654 7. V. M. MOCHO and F. X. OUF, “Clogging of industrial pleated high efficiency particulate air (HEPA)
655 filters in the event of fire,” *Nucl. Eng. Des.* **241** 5, 1785 (2011);
656 <https://doi.org/10.1016/j.nucengdes.2011.01.036>.
- 657 8. S. BOURROUS et al., “Measurement and modeling of pressure drop of HEPA filters clogged with
658 ultrafine particles,” *Powder Technol.* **289**, 109 (2016); <https://doi.org/10.1016/j.powtec.2015.11.020>.
- 659 9. T. ISHIBASHI et al., “Clogging of HEPA filters by soot during fire events in nuclear fuel cycle
660 facilities,” *Nucl. Technol.* **187**, 57 (2014).
- 661 10. J. G. QUINTIERE, “A Review of Experiments on the Airborne Release of Simulated Radioactive
662 Compounds from Fire,” *Fire Technol.* **34** 4, 307, Kluwer Academic Publishers (1998);
663 <https://doi.org/10.1023/A:1015314510914>.
- 664 11. F.-X. OUF et al., “Contribution to the study of particle resuspension kinetics during thermal degradation
665 of polymers,” *J. Hazard. Mater.* **250–251**, 298 (2013); <https://doi.org/10.1016/j.jhazmat.2013.01.060>.
- 666 12. F.-X. OUF et al., “Airborne release of hazardous micron-sized metallic/metal oxide particles during
667 thermal degradation of polycarbonate surfaces contaminated by particles: Towards a phenomenological
668 description,” *J. Hazard. Mater.* **384**, 121490 (2020); <https://doi.org/10.1016/j.jhazmat.2019.12.1490>.
- 669 13. Y. FERNANDEZ and P. BURGHOFFER, “Radioactive Aerosols Emission in Fires,” *Aerosol Sci.*
670 *Technol.* **23** 2, 231, Taylor & Francis Group (1995); <https://doi.org/10.1080/02786829508965306>.
- 671 14. M. Y. BALLINGER et al., “Aerosols Released in Accidents in Reprocessing Plants,” *Nucl. Technol.* **81**
672 **2**, 278 (1988); <https://doi.org/10.13182/NT88-A34097>.
- 673 15. L. BOUILLOUX, “Etude de la mise en suspension physico-chimique des oxydes de plutonium et
674 d’uranium lors de la combustion de polycarbonate et de ruthénium lors de la combustion des solvants de
675 retraitement du combustible irradié,” Institut national polytechnique de Grenoble (1998).
- 676 16. G. NISHIO and K. HASHIMOTO, “Release of radioactive materials in simulation tests of a postulated
677 solvent fire in a nuclear fuel reprocessing plant,” *Nucl. Technol.* **88**, 213 (1989).
- 678 17. J. MISHIMA and L. C. SCHWENDIMAN, “Some experimental measurements of airborne uranium
679 (representing plutonium) in transportation accidents.” (1973).
- 680 18. M. A. HALVERSON, M. Y. BALLINGER, and G. W. DENNIS, “Combustion Aerosols Formed During
681 Burning of Radioactively Contaminated Materials,” NUREG/CR 4736 (1987).
- 682 19. J. C. MALET et al., “Solvent pool fire testing,” in *Proceedings of the CSNI Specialist Meeting on*
683 *Interaction of Fire and Explosion with Ventilation Systems in Nuclear Facilities* **II** 83, pp. 391–404, Los
684 Alamos National Laboratory, Los Alamos, New Mexico (1983).
- 685 20. S. JORDAN and W. LINDNER, “Aerosols Released from Solvent Fire Accidents in Reprocessing
686 Plants,” Karlsruhe, Nucl. Energy Agency, 1984., 561pp. (1984).
- 687 21. H. D. SEEHARS, “Release of Pu-containing materials during a kerosene fire,” *J. Aerosol Sci.* **14** 3, 446
688 [https://doi.org/10.1016/0021-8502\(83\)90158-1](https://doi.org/10.1016/0021-8502(83)90158-1).
- 689 22. J. A. HUBBARD et al., “Airborne release fractions from surrogate nuclear waste fires containing
690 lanthanide nitrates and depleted uranium nitrate in 30% tributyl phosphate in kerosene,” *Nucl. Technol.*
691 **207** 1, 103, Taylor & Francis (2021); <https://doi.org/10.1080/00295450.2020.1739995>.
- 692 23. J. MISHIMA and L. C. SCHWENDIMAN, “Interim report: the fractional airborne release of dissolved
693 radioactive materials during the combustion of 30 percent normal tributylphosphate in a kerosine-type
694 diluent. BNWL-B-274.” (1973).
- 695 24. M. Y. BALLINGER and P. C. OWCZARSKI, “Radioactive source term models in a compartment fire
696 code,” *Nucl. Technol.* **69** 1, 36 (1985).

- 697 25. S. L. SUTTER, J. MISHIMA, and L. C. SCHWENDIMAN, "Fractional airborne release of strontium
698 during the combustion of 30 percent normal tributyl phosphate in a kerosene-type diluent" (1974).
- 699 26. S. JORDAN and W. LINDNER, "Aerosols released from solvent fire accidents in reprocessing plants,"
700 in Proceedings of the CSNI Specialist meeting on nuclear aerosols in reactor safety., pp. 101–108,
701 Karlsruhe, Federal Republic of Germany (1985).
- 702 27. J. MISHIMA and L. C. SCHWENDIMAN, "Interim report: the fractional airborne release of dissolved
703 radioactive materials during the combustion of 30 percent normal tributyl phosphate in a kerosene-type
704 diluent," Richland, WA (United States) (1973); <https://doi.org/10.2172/4296864>.
- 705 28. D. D. EVANS et al., "In Situ Burning of Oil Spills," *J. Res. Natl. Inst. Stand. Technol.* **106** 1, 231
706 (2001); <https://doi.org/10.6028/jres.106.009>.
- 707 29. Y. YAO et al., "Scale effect of mass loss rates for pool fires in an open environment and in tunnels with
708 wind," *Fire Saf. J.* **105** June 2018, 41, Elsevier Ltd (2019); <https://doi.org/10.1016/j.firesaf.2019.02.004>.
- 709 30. V. KOGAN and P. M. SCHUMACHER, "Plutonium Release Fractions from Accidental Fires," *Nucl.*
710 *Technol.* **161** 2, 190, American Nuclear Society (2008).
- 711 31. M. ŠULKA, L. CANTREL, and V. VALLET, "Theoretical Study of Plutonium(IV) Complexes Formed
712 within the PUREX Process: A Proposal of a Plutonium Surrogate in Fire Conditions," *J. Phys. Chem. A*
713 **118** 43, 10073 (2014); <https://doi.org/10.1021/jp507684f>.
- 714 32. H. FEUCHTER et al., "Influence of Light and Temperature on the Extractability of Cerium(IV) as a
715 Surrogate of Plutonium(IV) and its Effect on the Simulation of an Accidental Fire in the PUREX
716 Process," *ACS Omega* **4** 7, 12896 (2019); <https://doi.org/10.1021/acsomega.9b00746>.
- 717 33. P. A. BINGHAM et al., "The Use of Surrogates in Waste Immobilization Studies: A Case Study of
718 Plutonium," *MRS Proc.* **1107** 2006, 421 (2008); <https://doi.org/10.1557/PROC-1107-421>.
- 719 34. M. R. ANTONIO et al., "Third phase inversion, red oil formation, and multinuclear speciation of
720 tetravalent cerium in the tri-n-butyl phosphate–n-dodecane solvent extraction system," *Sep. Sci.*
721 *Technol.* **53** 12, 1834, Taylor & Francis (2018); <https://doi.org/10.1080/01496395.2017.1281303>.
- 722 35. A. L. BROWN et al., "Contaminant Entrainment from a Gasoline Pool Fire," in Fall 2015 Western
723 States Section of the Combustion Institute, pp. 1–20 (2015).
- 724 36. A. L. BROWN and D. L. Y. LOUIE, "Contaminant Entrainment in a Liquid Fuel Fire," in 1st Thermal
725 and Fluid Engineering Summer Conference, TFESC, pp. 1–13 (2015).
- 726 37. F. PIERCE et al., "Multicomponent Evaporation Effects on Particulate Release in a Liquid Fuel Fire"
727 (2017).
- 728 38. J. O. COSANDEY, A. GÜNTHER, and P. RUDOLF VON ROHR, "Transport of salts and micron-sized
729 particles entrained from a boiling water pool," *Exp. Therm. Fluid Sci.* **27** 8, 877 (2003);
730 [https://doi.org/10.1016/S0894-1777\(03\)00060-8](https://doi.org/10.1016/S0894-1777(03)00060-8).
- 731 39. P. MOEYAERT et al., "Experimental and modelling study of ruthenium extraction with tri-n-
732 butylphosphate in the purex process," *Chem. Eng. Sci.* **158** August 2016, 580, Elsevier (2017);
733 <https://doi.org/10.1016/j.ces.2016.10.035>.
- 734 40. W. L. COWLEY et al., "Estimating Risk Using Bounding Calculations and Limited Data," in American
735 Institute of Chemical Engineers, Spring Meeting (1999).
- 736 41. D. J. PRUETT, "The Solvent Extraction Behavior of Ruthenium I - The Nitric Acid-Tri-n-Butyl
737 Phosphate System.," *Radiochim. Acta* **27**, 115 (1980).
- 738 42. P. G. M. BROWN, J. M. FLETCHER, and A. G. WAIN, "Report AERE C/R 2260," Harwell, England
739 (1957).
- 740 43. D. O. C. SOUZA and F. C. MENEGALLI, "Image analysis: Statistical study of particle size distribution
741 and shape characterization," *Powder Technol.* **214** 1, 57, Elsevier B.V. (2011);
742 <https://doi.org/10.1016/j.powtec.2011.07.035>.
- 743 44. C. LEFEBVRE et al., "Speciation of Ruthenium in Organic TBP/TPH Organic Phases: A Study about
744 Acidity of Nitric Solutions," *Procedia Chem.* **21**, 54 (2016);
745 <https://doi.org/10.1016/j.proche.2016.10.008>.
- 746 45. Ž. PETROVIĆ et al., "Formation of RuO₂ nanoparticles by thermal decomposition of Ru(NO)(NO₃)₃,"
747 *Ceram. Int.* **41** 6, 7811 (2015); <https://doi.org/10.1016/j.ceramint.2015.02.115>.
- 748 46. P. H. DUVIGNEAUD and D. REINHARD-DERIE, "DTA study of RuO₂ formation from the thermal
749 decomposition of ruthenium(III) hydrate," *Thermochim. Acta* **51** 2–3, 307 (1981);
750 [https://doi.org/10.1016/0040-6031\(81\)85168-4](https://doi.org/10.1016/0040-6031(81)85168-4).
- 751 47. C. BRUNEAU et al., "Thermal degradation of tri-n-butyl phosphate," *J. Anal. Appl. Pyrolysis* **3** 1, 71
752 (1981); [https://doi.org/10.1016/0165-2370\(81\)80027-7](https://doi.org/10.1016/0165-2370(81)80027-7).
- 753 48. T. KOBYLINSKI and B. W. TAYLER, "Ruthenium phosphates as new compounds and process of using
754 same. US Patent 3,895,095" (1975).
- 755 49. A. DAGHETTI, G. LODI, and S. TRASATTI, "Interfacial properties of oxides used as anodes in the
756 electrochemical technology," *Mater. Chem. Phys.* **8** 1, 1 (1983); [25](https://doi.org/10.1016/0254-</p>
</div>
<div data-bbox=)

- 757 0584(83)90020-2.
- 758 50. H. LHUISSIER and E. VILLERMAUX, "Bursting bubble aerosols," *J. Fluid Mech.* **696**, 5 (2012);
759 <https://doi.org/10.1017/jfm.2011.418>.
- 760 51. A. BALDELLI et al., "Effect of crystallization kinetics on the properties of spray dried microparticles,"
761 *Aerosol Sci. Technol.* **50** 7, 693, Taylor & Francis (2016);
762 <https://doi.org/10.1080/02786826.2016.1177163>.
- 763 52. H. HIRAI et al., "Characterization and thermal behavior of amorphous rare earth phosphates," *J. Alloys*
764 *Compd.* **374** 1–2, 84 (2004); <https://doi.org/10.1016/j.jallcom.2003.11.069>.
- 765 53. I. ROMER et al., "Impact of particle size, oxidation state and capping agent of different cerium dioxide
766 nanoparticles on the phosphate-induced transformations at different pH and concentration," *PLoS One*
767 **14** 6, 1 (2019); <https://doi.org/10.1371/journal.pone.0217483>.
- 768 54. D. C. BLANCHARD and L. D. SYZDEK, "Film drop production as a function of bubble size," *J.*
769 *Geophys. Res.* **93** C4, 3649 (1988); <https://doi.org/10.1029/JC093iC04p03649>.
- 770 55. F. RESCH and G. AFETI, "Film drop distributions from bubbles bursting in seawater," *J. Geophys. Res.*
771 **96** C6, 10681 (1991); <https://doi.org/10.1029/91jc00433>.
- 772 56. J. WU, "Production Functions of Film Drops by Bursting Bubbles," *J. Phys. Oceanogr.* **31** 11, 3249
773 (2002); [https://doi.org/10.1175/1520-0485\(2001\)031<3249:pfofdb>2.0.co;2](https://doi.org/10.1175/1520-0485(2001)031<3249:pfofdb>2.0.co;2).
- 774 57. M. K. KOCH et al., "Radionuclide re-entrainment at bubbling water pool surfaces," *J. Aerosol Sci.* **31** 9,
775 1015 (2000); [https://doi.org/10.1016/S0021-8502\(00\)00025-2](https://doi.org/10.1016/S0021-8502(00)00025-2).
- 776 58. D. C. BLANCHARD, "The Ejection of Drops from the Sea and Their Enrichment with Bacteria and
777 Other Materials: A Review," *Estuaries* **12** 3, 127 (1989); <https://doi.org/10.2307/1351816>.
- 778 59. D. E. SPIEL, "On the births of film drops from bubbles bursting on seawater surfaces," *J. Geophys. Res.*
779 *Ocean.* **103** C11, 24907 (1998); <https://doi.org/10.1029/98JC02233>.
- 780 60. L. M. RUSSELL and E. G. SINGH, "Submicron salt particle production in bubble bursting," *Aerosol*
781 *Sci. Technol.* **40** 9, 664 (2006); <https://doi.org/10.1080/02786820600793951>.
- 782 61. W. R. KE et al., "Characterization of aerosol emissions from single bubble bursting," *J. Aerosol Sci.* **109**
783 March, 1, Elsevier Ltd (2017); <https://doi.org/10.1016/j.jaerosci.2017.03.006>.
- 784 62. R. BORKOWSKI, H. BUNZ, and W. SCHÖCK, "Resuspension of fission products during severe
785 accidents in light-water reactors. KfK 3987, EUR 10391EN." (1986).
- 786 63. T. WONGSAWA et al., "The experimental investigations on viscosity, surface tension, interfacial
787 tension and solubility of the binary and ternary systems for tributyl phosphate (TBP) extractant in
788 various organic solvents with water: Thermodynamic NRTL model and molecular inte," *J. Mol. Liq.*
789 **251**, 229, Elsevier B.V. (2018); <https://doi.org/10.1016/j.molliq.2017.12.074>.
- 790 64. P. KULKARNI, P. A. BARON, and K. WILLEKE, *Aerosol Measurement: Principles, Techniques, and*
791 *Applications: Third Edition*, in *Aerosol Measurement: Principles, Techniques, and Applications: Third*
792 *Edition* (2011); <https://doi.org/10.1002/9781118001684>.
- 793

794 **Supplementary information SI-1: yield of digestion associated to ICP analysis**

795
 796 Figure SI-1 presents the evolution of ICP-MS detection yield Y_{ICP} of cerium as a function of mass of CeO_2 particles
 797 ($5 \mu m$ CeO_2 powder, REacton®, 99.9% reference 215-150-4 from Alfa Aesar) deposited on reference samples.
 798 For this purpose, cellulose acetate membranes similar to those used for sampling during HTP/TBP pool fire
 799 experiments were considered. CeO_2 powder were aerosolized using a vortex shaker device¹ and mass of deposited
 800 particles was determined by weighing according to NF ISO 15767². ICP-MS analysis was carried out by Intertek
 801 laboratory using previously qualified digestion protocol. The detection yield Y_{ICP} both includes digestion and
 802 detection yields and is defined as the ratio between the mass of cerium determined by ICP analysis m_{ICP}^{Ce} and the
 803 mass of cerium deposited on the reference membrane m_{ref}^{Ce}
 804

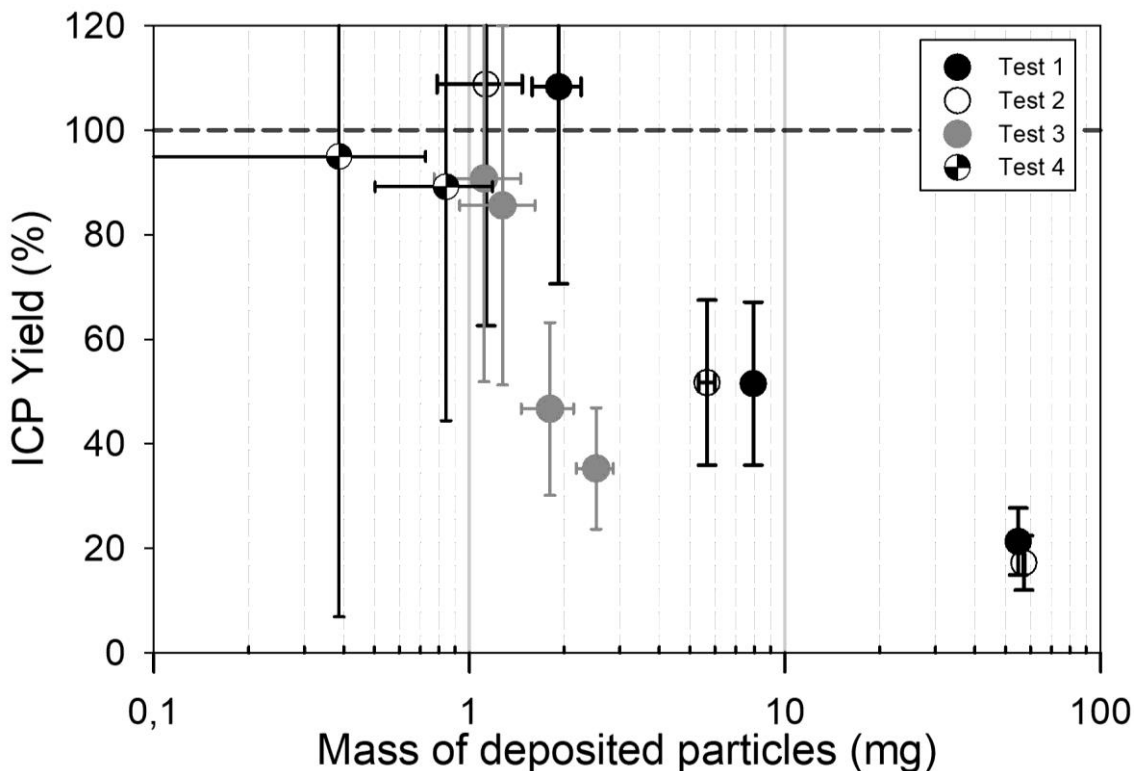
805
$$Y_{ICP}^{chemical\ form\ of\ Ce} = Y_{detection\ ICP-MS}^{chemical\ form\ of\ Ce} \cdot Y_{digestion}^{chemical\ form\ of\ Ce} = \frac{m_{ICP}^{Ce}}{m_{ref}^{Ce}}$$

806
 807 The corresponding uncertainty is defined as:
 808

809
$$u(R_m) = \sqrt{\left(\frac{1}{m_{ref}^{Ce}}\right)^2 \cdot u^2(m_{ICP}^{Ce}) + \left(\frac{-m_{ICP}^{Ce}}{(m_{ref}^{Ce})^2}\right) \cdot u^2(m_{ref}^{Ce})}$$

810
 811 with $u(m_{ICP}^{Ce})$ and $u(m_{ref}^{Ce})$ the uncertainties associated to the ICP and reference masses, determined according to
 812 NF ISO 15767.

813 It is worth noting that ICP yields are close to 100 % for reference mass lower than 2 mg and decreases for larger
 814 deposited mass. This decrease is not relevant for our fire samples since, according to the initial mass and ARF,
 815 less than 0.1 mg of cerium particles is expected on membranes. Mean ICP yield of 89.3 % +/- 6.5 % was determined
 816 for deposited mass in the range 0.4 – 2 mg and was considered as a correction factor in the computation of ARF.
 817



818
 819
 820 Figure SII-1: digestion yield of cerium reference samples
 821

¹ Gensdarmes, F., & Roynette, A. (2013). French patent: W02013092816.

² AFNOR. (2008). NF ISO 15767. Atmosphères des lieux de travail - Contrôle et caractérisation des erreurs de pesée des aérosols collectés.

822 **Supplementary information SI-2: calibration of XRF for samples containing ruthenium**

823

824 Figure SI-2 presents the experimental calibration curve between mass of ruthenium and number of events recorded
 825 for an X-ray energy of 19.279 keV corresponding to the K_{α} emission ray of Ruthenium. RuO_2 particles were
 826 deposited on acetate cellulose membrane using a vortex shaker³. Mass of deposited Ruthenium particles was
 827 determined by weighing according to NF ISO 15767⁴. Mass of ruthenium is then linked to number $Nb_{events\ K_{\alpha}}$ of
 828 K_{α} events according to the following relation and a calibration factor C_f :

829

830

$$m_{Ru} = C_f \cdot Nb_{events\ K_{\alpha}}$$

831

832 The corresponding uncertainty is defined as:

833

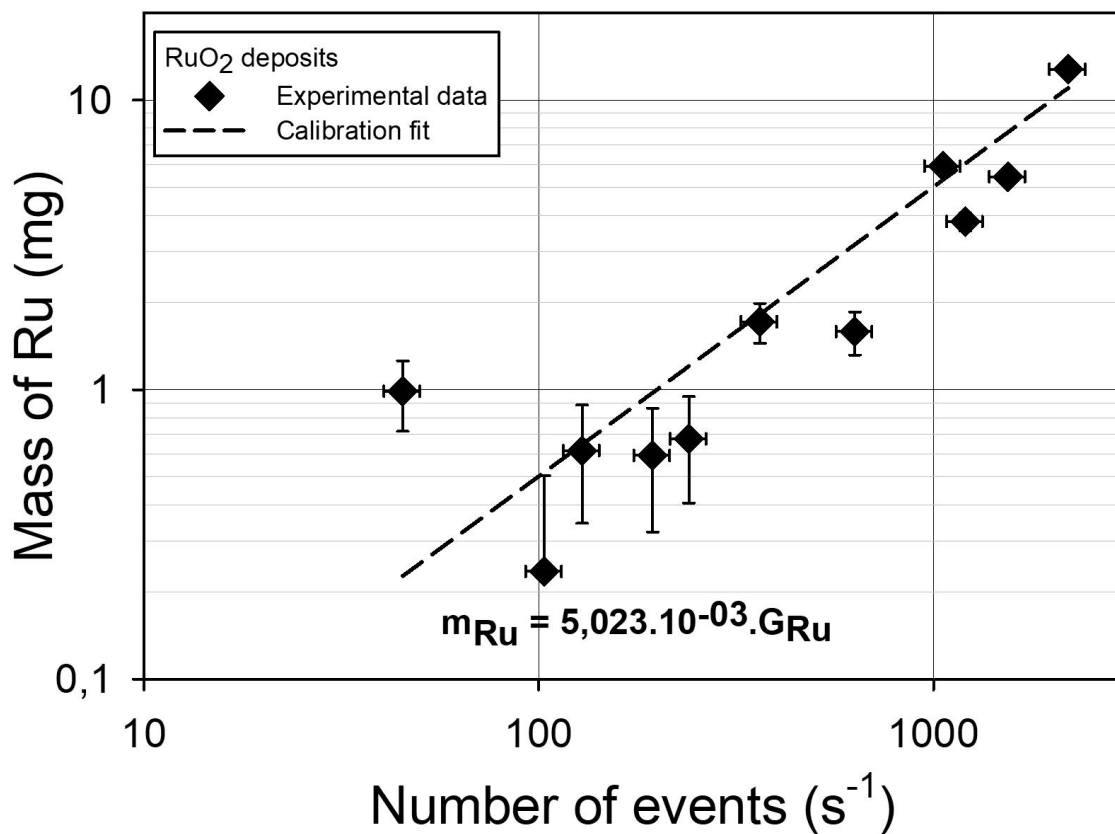
834

$$u(m_{Ru}) = \sqrt{Nb_{events\ K_{\alpha}}^2 \cdot u^2(C_f) + C_f^2 \cdot u^2(Nb_{events\ K_{\alpha}})},$$

835

836 with $u(C_f)$ and $u(Nb_{events\ K_{\alpha}})$ the uncertainties associated to the calibration factor (determined from the linear fit)
 837 and number of events according to the spectrometer specifications.

838



839

840 Figure SI2-1: experimental calibration curve linking mass of ruthenium with number of events recorded by X-
 841 ray spectrometer for the K_{α} Ruthenium energy (19.279 keV⁵)

842

³ Gensdarmes, F., & Roynette, A. (2013). French patent: W02013092816.

⁴ AFNOR. (2008). NF ISO 15767. Atmosphères des lieux de travail - Contrôle et caractérisation des erreurs de pesée des aérosols collectés.

⁵ <http://xdb.lbl.gov/>

843 **Supplementary information SI-3: computation of ARF experimental uncertainties associated**

844

845 Airborne release fraction ARF is defined as:

846
$$ARF = \frac{m_{\text{element}}^{\text{sampling}}}{m_{\text{element}}^{\text{initial}} \cdot P_{P(\%)} \cdot F_{P(\%)}}$$

847 Corresponding uncertainty could be computed according to:

848
$$u(ARF) = \sqrt{\left(\frac{\partial ARF}{\partial m_{\text{element}}^{\text{sampling}}}\right)^2 u^2(m_{\text{element}}^{\text{sampling}}) + \left(\frac{\partial ARF}{\partial m_{\text{element}}^{\text{initial}}}\right)^2 u^2(m_{\text{element}}^{\text{initial}}) + \left(\frac{\partial ARF}{\partial P_{P(\%)}}\right)^2 u^2(P_{P(\%)}) + \left(\frac{\partial ARF}{\partial F_{P(\%)}}\right)^2 u^2(F_{P(\%)})}$$

849 Uncertainty associated to the sampled mass of element of interest $u(m_{\text{element}}^{\text{sampling}})$ is determined for cerium according
850 to ICP measurement uncertainty (see SI-1) and for ruthenium according to X-Ray Fluorescence measurement
851 uncertainty (see SI-2).

852 Uncertainty associated to initial mass of element of interest $u(m_{\text{element}}^{\text{initial}})$ is determined according to the preparation
853 protocol of contaminated solvents. First, a known mass of salt containing the element of interest $m_{\text{aqueous}}^{\text{initial}}$ was first
854 dissolved in a known volume of aqueous HNO_3 solution. The corresponding mass of element in the aqueous phase
855 is then defined from the mass of dissolved salt m_{salt} and the contribution of the element of interest to the
856 composition of this salt $\%_{\text{element/salt}}$:

857

858
$$m_{\text{element}}^{\text{aqueous}} = m_{\text{salt}} \cdot \%_{\text{element/salt}}$$

859

860 Uncertainty associated to the composition of the salt was assumed negligible and uncertainty associated to the
861 mass of salt was only considered to compute the uncertainty corresponding to the mass of element of interest in
862 the aqueous phase:

863
$$u(m_{\text{element}}^{\text{aqueous}}) = u(m_{\text{salt}}) \cdot \%_{\text{element/salt}}$$

864

865 The mass of element of interest in HTP/TBP is defined as a function of the mass of this element in the aqueous
866 phase $m_{\text{element}}^{\text{aqueous}}$ in contact with the organic phase during the extraction protocol presenting an extraction coefficient
867 $C_{\text{ext, element}}$ for this element:

868
$$u(m_{\text{element}}^{\text{initial}}) = m_{\text{element}}^{\text{aqueous}} \cdot C_{\text{ext, element}}$$

869

870 Uncertainty of this initial mass of element in the organic phase is computed according to:

871

872
$$u(m_{\text{element}}^{\text{initial}}) = \sqrt{\left(\frac{\partial m_{\text{element}}^{\text{initial}}}{\partial m_{\text{element}}^{\text{aqueous}}}\right)^2 u^2(m_{\text{element}}^{\text{aqueous}}) + \left(\frac{\partial m_{\text{element}}^{\text{initial}}}{\partial C_{\text{ext, element}}}\right)^2 u^2(C_{\text{ext, element}})}$$

873 Uncertainty associated to the extraction coefficient was determined for cerium from experimental determination
874 of this coefficient³² and for ruthenium by considering mean values and corresponding standard deviation computed
875 from experimental values reported in previous studies (TBP in contact, under ambient conditions, during 60
876 minutes with HNO_3 3 M aqueous phase containing dissolved Ruthenium Nitrosyl Nitrate salt^{15,41}).

877 The volume fraction of gas sampled through the membrane $P_{P(\%)}$ is defined as the ratio between the volumetric
878 flow rate sampled Q_{sampled} and the volumetric flow rate within the test bench exhaust duct Q_{exhaust} :

879

879
$$P_{P(\%)} = Q_{\text{sampled}} / Q_{\text{exhaust}}$$

880 Mass flow regulator was used to maintain the sampled flow rate then uncertainty associated to this flowrate was
881 assumed negligible. The exhaust duct flow rate was manually regulated during each test and a mean exhaust flow
882 rate was then computed and considered. Corresponding standard deviation associated to this mean exhaust flow
883 rate was considered as the Q_{exhaust} uncertainty $u(Q_{\text{exhaust}})$. Finally, the $P_{P(\%)}$ uncertainty is defined as follow:

884
$$u(P_{P(\%)}) = \sqrt{\left(-\frac{Q_{\text{sampled}}}{Q_{\text{exhaust}}^2}\right) u^2(Q_{\text{exhaust}})}$$

885

886 Finally, penetration fraction $F_{P(\%)}$ was fixed, according to computations reported in our previous study¹², at a
887 value of 1 (no losses of particles in the test bench) for aerodynamic diameter lower than 5 μm .

888 **Supplementary information SI-4: values of airborne release fractions measured for each experimental**
 889 **conditions**
 890

891 Table SI-I: ARF values determined for each Ce(+III) contaminated HTP/TBP solutions

Fuel composition (in volume)	Contaminant	Salt	V _{org} / V _{aq} (ml)	[Cont _{org}] (g/L)	ARF (%)
Contaminated 70% HTP / 30% TBP	Ce(+III)	Cerium nitrate hexahydrate Ce(NO ₃) ₃ .6(H ₂ O)	30 / 0	0.2	0.30 +/- 0.10
					0.79 +/- 0.21
					0.67 +/- 0.17
				4.8	0.70 +/- 0.06
					3.07 +/- 0.24
					0.92 +/- 0.07
				9.5	0.12 +/- 0.01
					0.04 +/- 0.004
					0.06 +/- 0.01
				8.6	0.66 +/- 0.05
Contaminated 70% HTP / 30% TBP + Pure HNO ₃ 3M, Ratio 1:1			15 / 15	0.4	5.32 +/- 0.66
					3.81 +/- 0.47
					3.59 +/- 0.45
				8.6	1.35 +/- 0.17
					2.21 +/- 0.28

892
 893
 894
 895
 896
 897
 898
 899
 900
 901

902 Table SI-II: ARF values determined for each Ce(+IV) contaminated HTP/TBP solutions

Fuel composition (in volume)	Contaminant	Salt	V _{org} / V _{aq} (ml)	[Cont _{org}] (g/L)	ARF (%)
Contaminated 70% HTP / 30% TBP	Ce(+IV)	Cerium(IV) Ammonium Nitrate (NH ₄) ₂ Ce(NO ₃) ₆	30 / 0	9.7	0.01 +/- 0.001
					0.05 +/- 0.01
					0.03 +/- 0.004
				10.2	0.12 +/- 0.03
					0.28 +/- 0.06
					0.20 +/- 0.04
					0.20 +/- 0.04
					0.18 +/- 0.04
					0.33 +/- 0.07
					0.55 +/- 0.12
Contaminated 70% HTP / 30% TBP + Pure HNO ₃ 3M, Ratio 1:1	Ce(+IV)	Cerium(IV) Ammonium Nitrate (NH ₄) ₂ Ce(NO ₃) ₆	15 / 15	9.7	0.27 +/- 0.03
					0.16 +/- 0.02
					0.19 +/- 0.02
				10.2	0.45 +/- 0.06
					0.58 +/- 0.08
					1.18 +/- 0.15
					2.28 +/- 0.49
					1.97 +/- 0.43
					1.32 +/- 0.29
					1.69 +/- 0.37

903

904

905

906

907

908 Table SI-III: ARF values determined for each Ru(+III) contaminated HTP/TBP solutions

Fuel composition (in volume)	Contaminant	Salt	V _{org} / V _{aq} (ml)	[Cont _{org}] (g/L)	ARF (%)
Contaminated 70% HTP / 30% TBP	Ru(+III)	Ruthenium(III) Nitrosylnitrate RuNO(NO ₃) ₃	30 / 0	0.6	0.63 +/- 0.18
					1.81 +/- 0.40
					0.53 +/- 0.18
Contaminated 70% HTP / 30% TBP + Pure HNO ₃ 3M, Ratio 1:1			15 / 15		10.35 +/- 7.49
					19.58 +/- 16.04
					7.29 +/- 1.16

909

910

911

912

913

914

915

916

917

918